Electronic Supplementary Material (ESI) for Dalton Transactions.
This journal is © The Royal Society of Chemistry 2024

Electronic Supplementary Information

Synthesis and luminescent properties of Ru(II)/Au(I) or Ir(III)/Au(I) hetero-bimetallic and hetero-trimetallic complexes

Richard C. Knighton[a] and Simon J. A. Pope[a]*

[a] School of Chemistry, Main Building, Cardiff University, Cardiff CF10 3AT, Cymru/ Wales, UK. E-mail: popesj@cardiff.ac.uk

Figure S1. ^{1}H NMR spectrum (300 MHz, 293 K, $CDCl_3$) of dimeric $[Ir(Me_3quinox)_2(\mu_2\text{-}Cl)]_2$. **3**
Figure S2. ^{1}H NMR spectrum of $[Ir(Me_3quinox)_2(MeCN)_2][PF_6]$ (500 MHz, 293 K, CD_3CN) **3**
Figure S3. $^{13}C\{^{1}H\}$ NMR spectrum of $[Ir(Me_3quinox)_2(MeCN)_2][PF_6]$ (500 MHz, 293 K, CD_3CN). **4**
Figure S4. HRMS of $[Ir(Me_3quinox)_2(MeCN)_2][PF_6]$ (ES+). (Top - theoretical; bottom - experimental). **4**
Figure S5. ^{1}H NMR spectrum of $[Ir(Me_3quinox)_2(bipy\text{-}Im1)][PF_6]_2$ (500 MHz, 293 K, CD_3CN). **5**
Figure S6. $^{13}C\{^{1}H\}$ NMR spectrum of $[Ir(Me_3quinox)_2(bipy\text{-}Im1)][PF_6]_2$ (126 MHz, 293 K, CD_3CN). **5**
Figure S7. HRMS of $[Ir(Me_3quinox)_2(bipy\text{-}Im1)][PF_6]_2$ (ES+). (Top - theoretical; bottom – experimental) **6**
Figure S8. ^{1}H NMR spectrum of $[Ir(Me_3quinox)_2(bipy\text{-}Im2)][PF_6]_3$ (500 MHz, 293 K, CD_3CN). **6**
Figure S9. $^{13}C\{^{1}H\}$ NMR spectrum of $[Ir(Me_3quinox)_2(bipy\text{-}Im2)][PF_6]_3$ (126 MHz, 293 K, CD_3CN). **7**
Figure S10. HRMS of $[Ir(Me_3quinox)_2(bipy\text{-}Im2)][PF_6]_3$ (ES+). (Top - theoretical; bottom - experimental). **7**
Figure S11. ^{1}H NMR spectrum of $[Ru\text{-}Au][PF_6]_3$ (500 MHz, 293 K, CD_3CN). **8**
Figure S12. $^{13}C\{1H\}$ NMR spectrum of $[Ru\text{-}Au][PF_6]_3$ (126 MHz, 293 K, CD_3CN). **8**
Figure S13. $^{31}P\{^{1}H\}$ NMR spectrum of $[Ru\text{-}Au][PF_6]_3$ (202 MHz, 293 K, CD_3CN). **9**
Figure S14. HRMS of $[Ru\text{-}Au][PF_6]_3$ (ES+). (Top - theoretical; bottom - experimental). **9**
Figure S15. ^{1}H NMR spectrum of $[Ru\text{-}Au_2][PF_6]_4$ (500 MHz, 293 K, CD_3CN). **10**
Figure S16. $^{13}C\{^{1}H\}$ NMR spectrum of $[Ru\text{-}Au_2][PF_6]_4$ (126 MHz, 293 K, CD_3CN). **10**
Figure S17. $^{31}P\{^{1}H\}$ NMR spectrum of $[Ru\text{-}Au_2][PF_6]_4$ (202 MHz, 293 K, CD_3CN). **11**
Figure S18. HRMS of $[Ru\text{-}Au_2][PF_6]_4$ (ES+). (Top - theoretical; bottom - experimental) **11**
Figure S19. ^{1}H NMR spectrum of $[Ir\text{-}Au][PF_6]_2$ (500 MHz, 293 K, CD_3CN). **12**
Figure S20. $^{13}C\{^{1}H\}$ NMR spectrum of $[Ir\text{-}Au][PF_6]_2$ (126 MHz, 293 K, CD_3CN). **12**
Figure S21. $^{31}P\{1H\}$ NMR spectrum of [Ir-Au][PF6]2 (202 MHz, 293 K, CD3CN). **13**
Figure S22. HRMS of [Ir-Au][PF6]2 (ES+). (Top - theoretical; bottom - experimental). **13**
Figure S23. ^{1}H NMR spectrum of $[Ir\text{-}Au_2][PF_6]_3$ (500 MHz, 293 K, CD_3CN). **14**
Figure S24. $^{13}C\{^{1}H\}$ NMR spectrum of $[Ir\text{-}Au_2][PF_6]_3$ (126 MHz, 293 K, CD_3CN). **14**
Figure S25. $^{31}P\{^{1}H\}$ NMR spectrum of $[Ir\text{-}Au_2][PF_6]_3$ (202 MHz, 293 K, CD_3CN). **15**
Figure S26. HRMS of $[Ir\text{-}Au_2][PF_6]_3$ (ES+). (Top - theoretical; bottom - experimental). **15**
Table S1. Crystals data and structure refinement for $[Ir(Me_3quinox)_2(MeCN)_2][BF_4]$ **16**
Figure S28. Single crystal X-ray structure of $[Ir(Me_3quinox)_2(MeCN)_2][BF_4]$ (ellipsoids plotted at the 50% probability level; H-atoms and counter anions omitted for clarity) **17**
Figure S29. Single crystal X-ray structure of $[Ir(Me_3quinox)_2(MeCN)_2][BF_4]$ (ellipsoids plotted at the 50% probability level; counter anions omitted for clarity) **17**
Figure S30. Unit cell packing of $[Ir(Me_3quinox)_2(MeCN)_2][BF_4]$ (ellipsoids plotted at the 50% probability level) **18**

Table S2. Crystals data and structure refinement for $[Ir(Me_3quinox)_2(bipy\text{-}Im2)][PF_6]_3$ **18**
Figure S32. Single crystal X-ray structure of $[Ir(Me_3quinox)_2(bipy\text{-}Im2)][PF_6]_3$ (ellipsoids plotted at the 50% probability level; counter anions omitted for clarity) **19**
Figure S33. Single crystal X-ray structure of $[Ir(Me_3quinox)_2(bipy\text{-}Im2)][PF_6]_3$ (ellipsoids plotted at the 50% probability level) **19**
Figure S34. Unit cell packing of $[Ir(Me_3quinox)_2(bipy\text{-}Im2)][PF_6]_3$ (ellipsoids plotted at the 50% probability level) **20**
Figure S35. Single crystal X-ray structure of $[Ru\text{-}Au][PF_6]_3$ (ellipsoids plotted at the 50% probability level; counter anions and disorder omitted for clarity) **21**
Figure S36. Single crystal X-ray structure of $[Ru\text{-}Au][PF_6]_3$ (ellipsoids plotted at the 50% probability level; counter anions omitted for clarity) **21**
Figure S37. Unit cell packing of $[Ru\text{-}Au][PF_6]_3$ (ellipsoids plotted at the 50% probability level) **22**
Table S3. Crystal data and structure refinement for $[Ru\text{-}Au)][PF_6]_3$ **22**
Table S5**.** Bond metrics for $[Ru\text{-}Au]\text{-}PF_6]_3$ **23**
Figure S38. Absorption spectra for the polycationic iridium complexes (293 K, aerated MeCN, 10^{-5} M). **23**
Table S6. Electrode oxidation potentials of the family of homo- and heterometallic complexes (mV shifts presented in parentheses) **24**
Figure S39. Cyclic voltammograms for the family of monometallic Ir/Ru heteropolymetallic Ir/Ru-Au complexes **24**
References **25**
25

S1 NMR and high-resolution mass spectra

S1.1 $[Ir(Me_3quinox)_2(\mu_2\text{-}Cl)]_2$

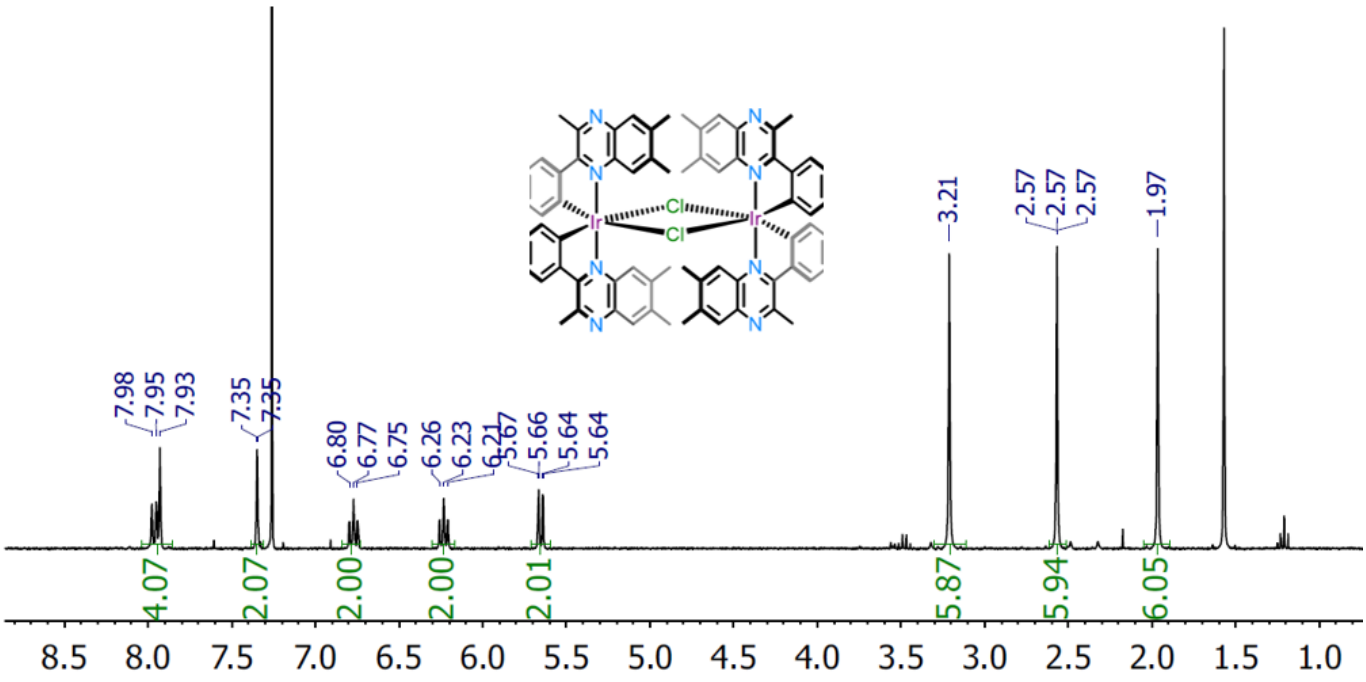

Figure S1. ^{1}H NMR spectrum (300 MHz, 293 K, $CDCl_3$) of dimeric $[Ir(Me_3quinox)_2(\mu_2\text{-}Cl)]_2$.

S1.2 $[Ir(Me_3quinox)_2(MeCN)_2][PF_6]$

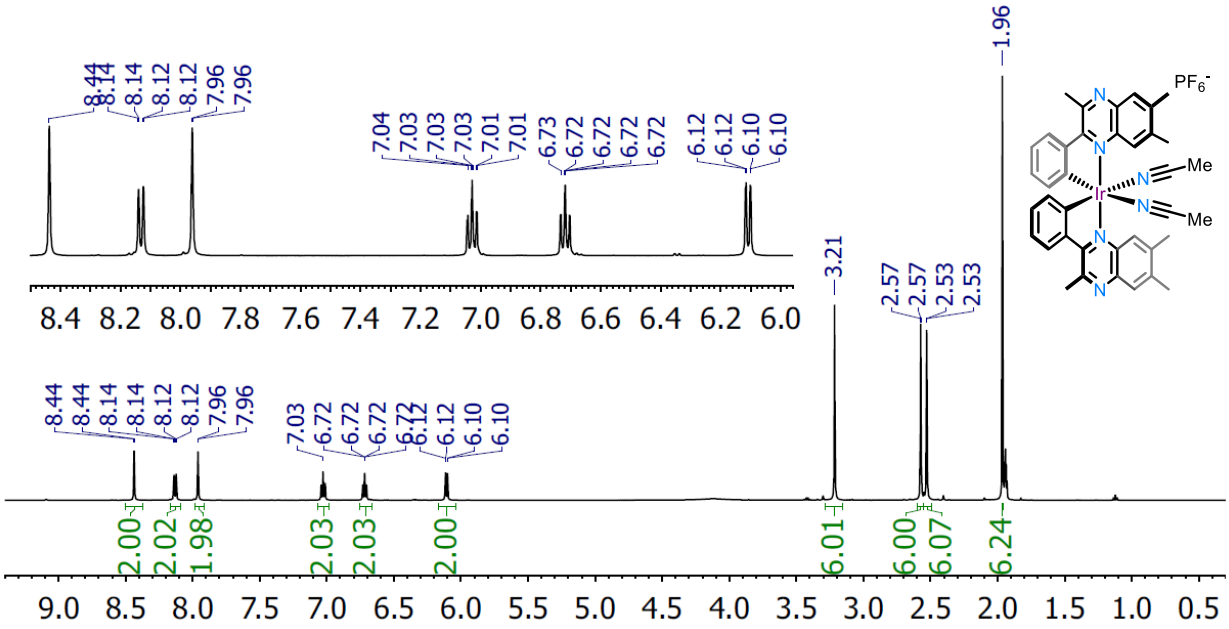

Figure S2. ^{1}H NMR spectrum of $[Ir(Me_3quinox)_2(MeCN)_2][PF_6]$ (500 MHz, 293 K, CD_3CN).

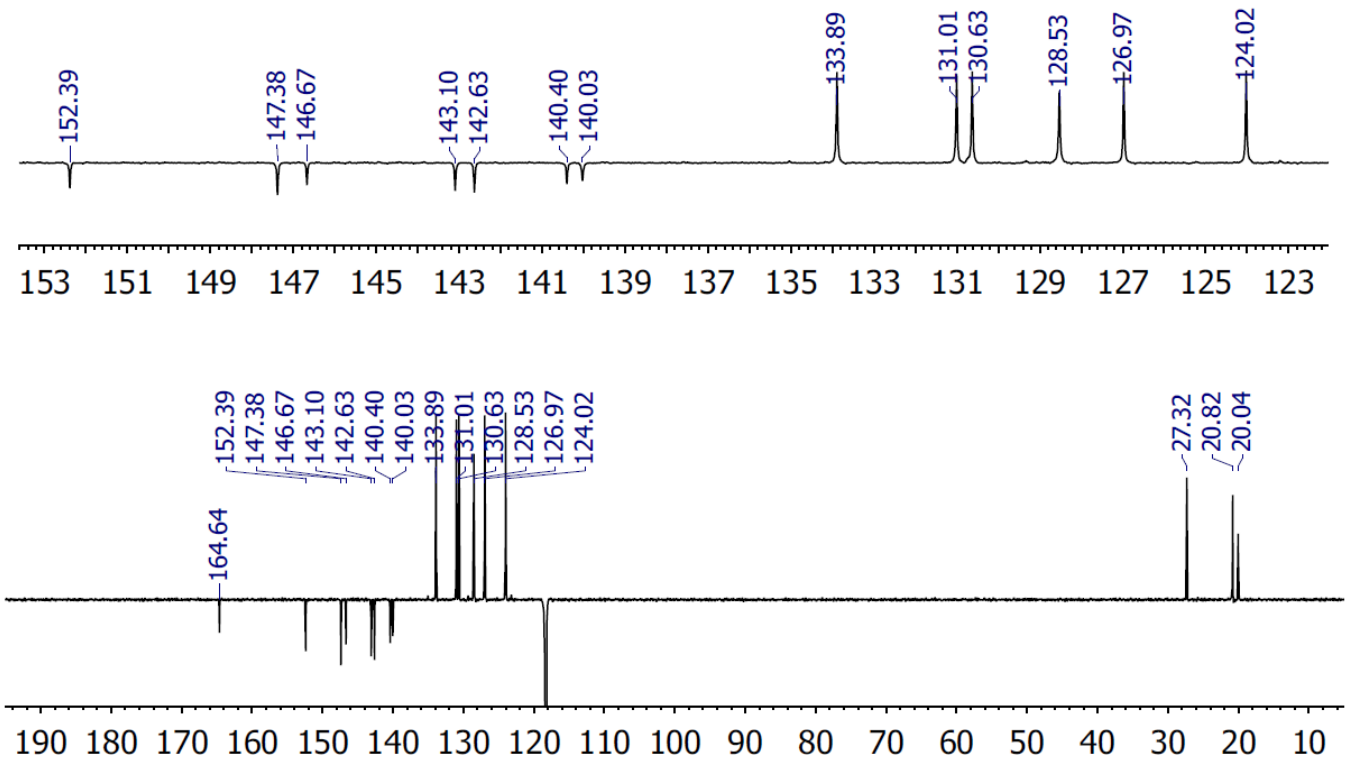

Figure S3. $^{13}C\{^{1}H\}$ NMR spectrum of $[Ir(Me_3quinox)_2(MeCN)_2][PF_6]$ (500 MHz, 293 K, CD_3CN).

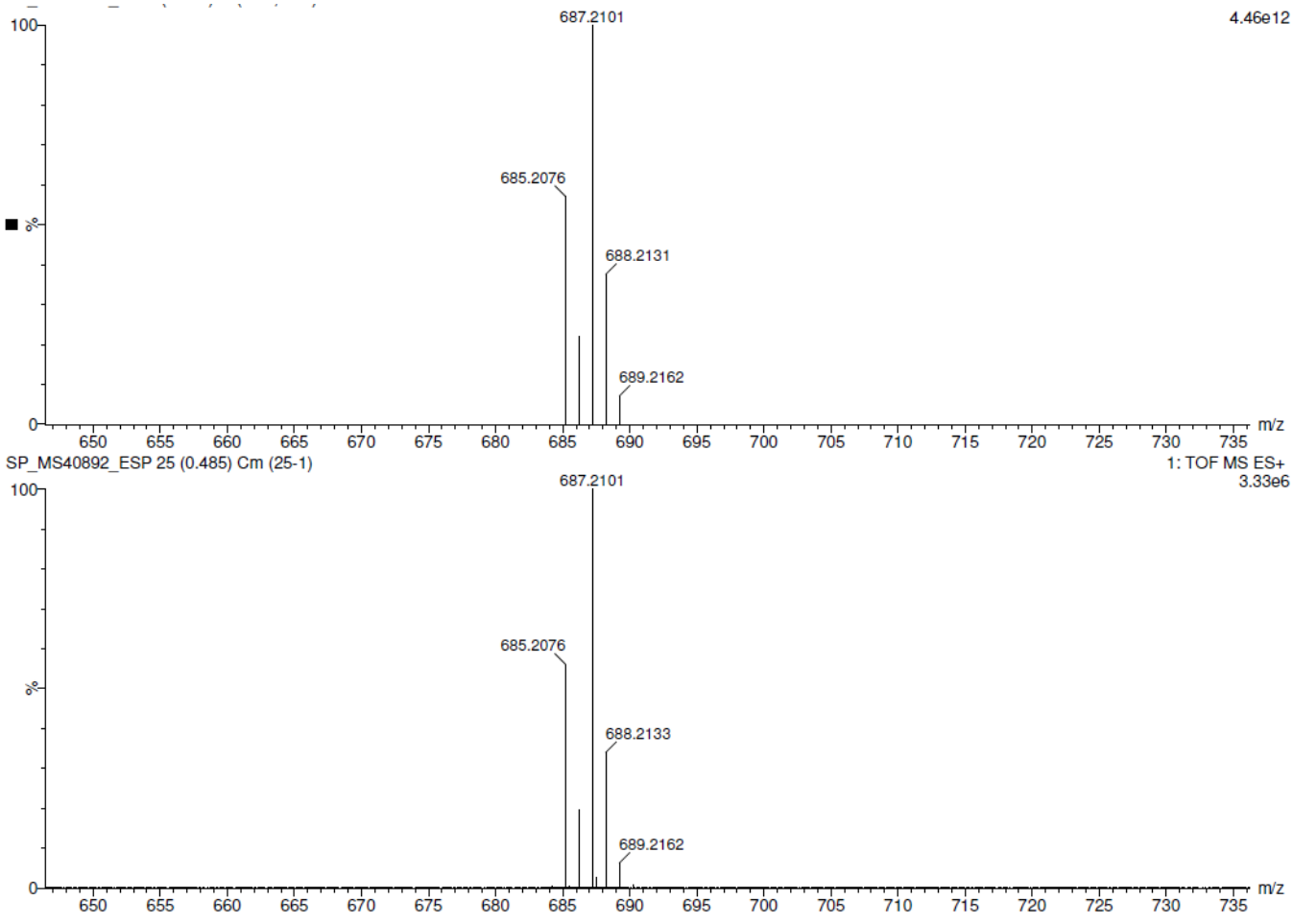

Figure S4. HRMS of $[Ir(Me_3quinox)_2(MeCN)_2][PF_6]$ (ES+). (Top - theoretical; bottom - experimental).

S1.3 [Ir(Me$_3$quinox)$_2$(bipy-Im1)][PF$_6$]$_2$

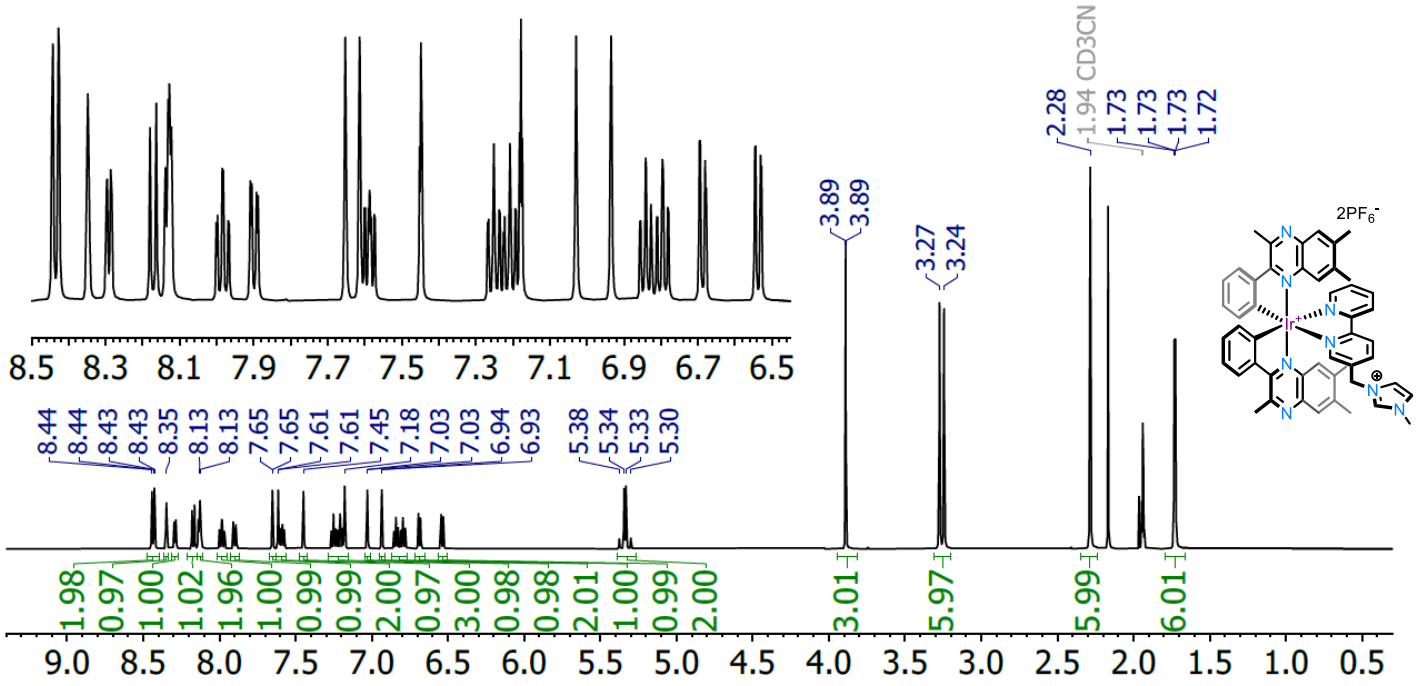

Figure S5. ^{1}H NMR spectrum of [Ir(Me$_3$quinox)$_2$(bipy-Im1)][PF$_6$]$_2$ (500 MHz, 293 K, CD$_3$CN).

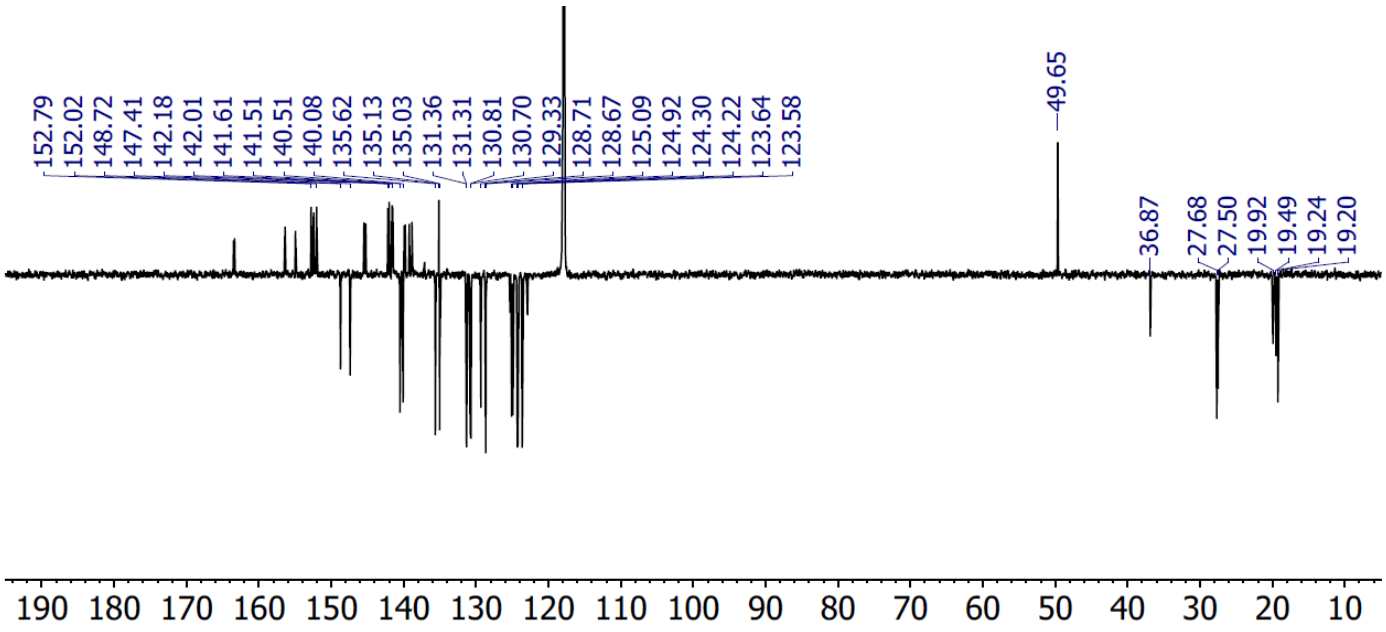

Figure S6. ^{13}C{^{1}H} NMR spectrum of [Ir(Me$_3$quinox)$_2$(bipy-Im1)][PF$_6$]$_2$ (126 MHz, 293 K, CD$_3$CN).

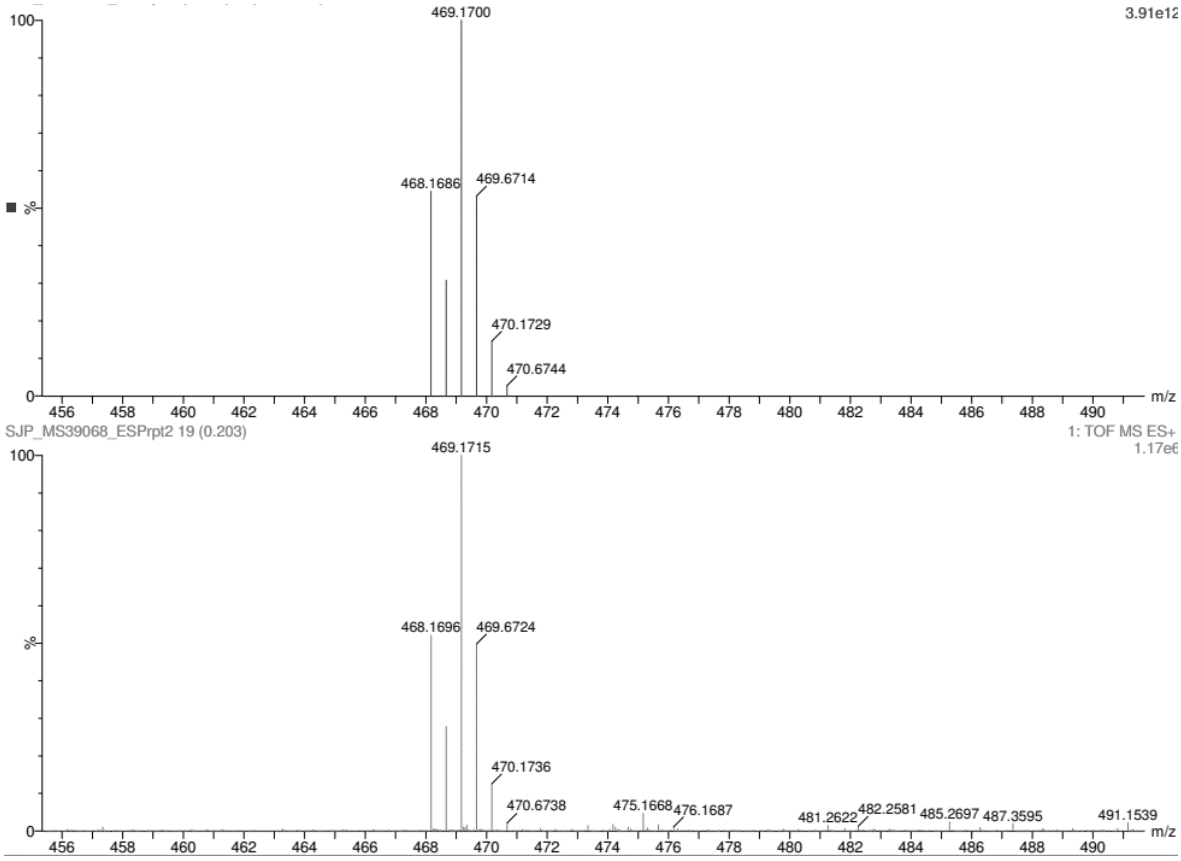

Figure S7. HRMS of $[Ir(Me_3quinox)_2(bipy\text{-}Im1)][PF_6]_2$ (ES+). (Top - theoretical; bottom - experimental).

S1.3 $[Ir(Me_3quinox)_2(bipy\text{-}Im2)][PF_6]_3$

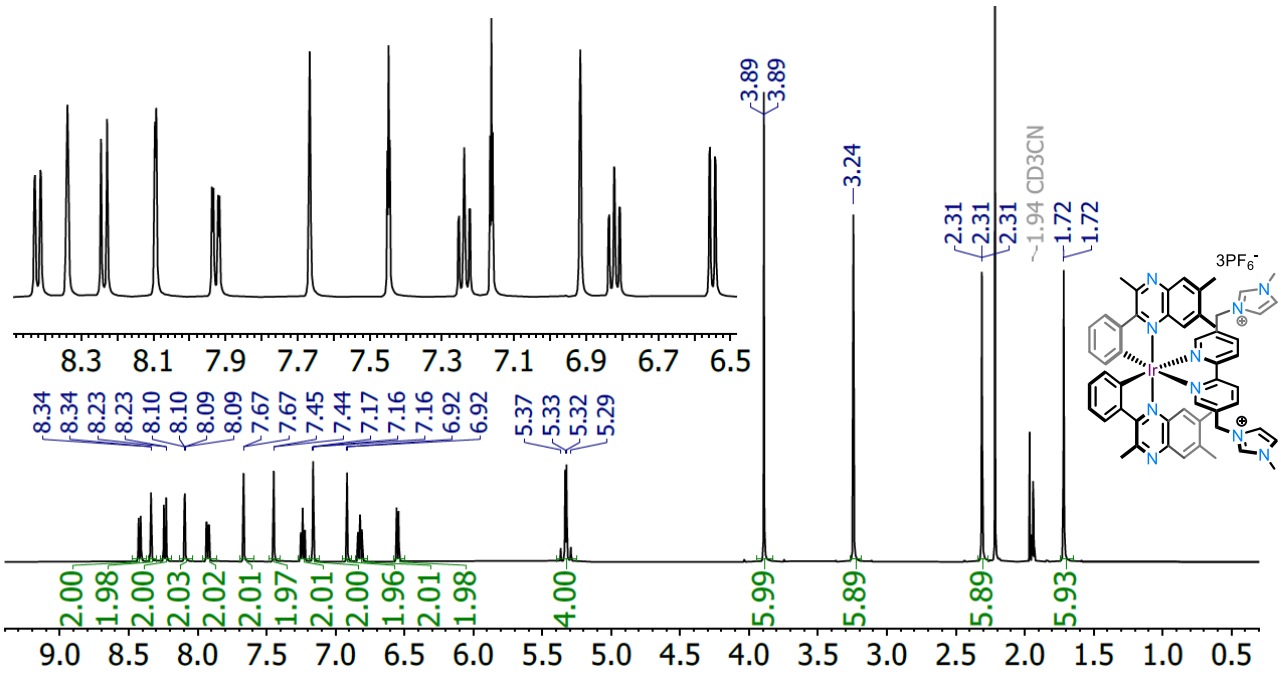

Figure S8. ^1H NMR spectrum of $[Ir(Me_3quinox)_2(bipy\text{-}Im2)][PF_6]_3$ (500 MHz, 293 K, CD_3CN).

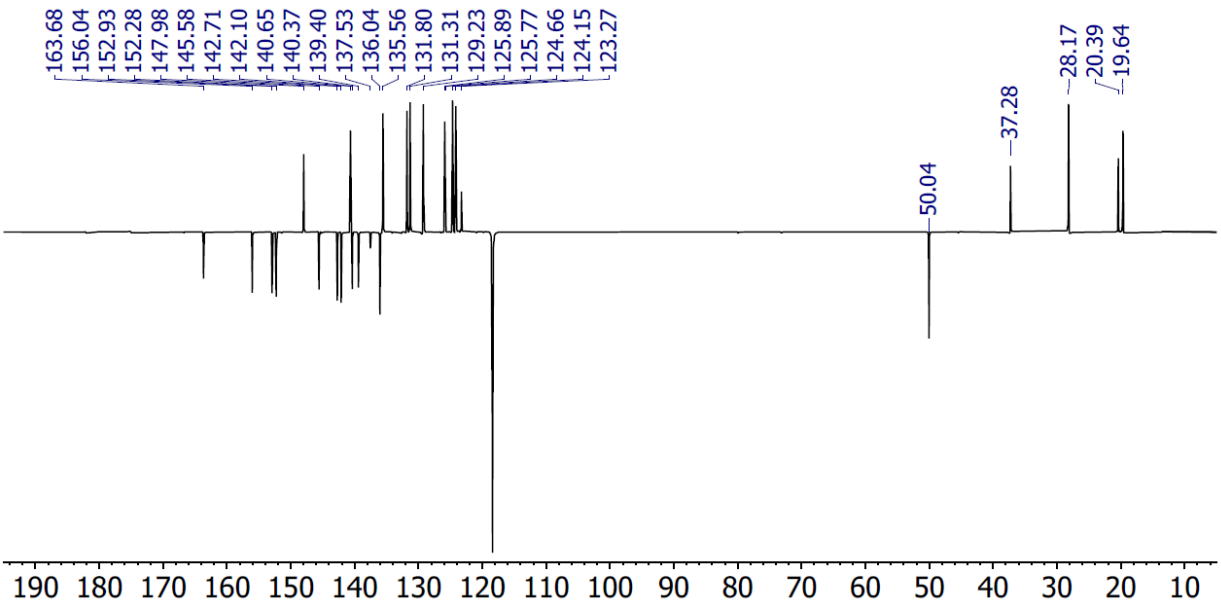

Figure S9. $^{13}C\{^{1}H\}$ NMR spectrum of $[Ir(Me_3quinox)_2(bipy\text{-}Im2)][PF_6]_3$ (126 MHz, 293 K, CD_3CN).

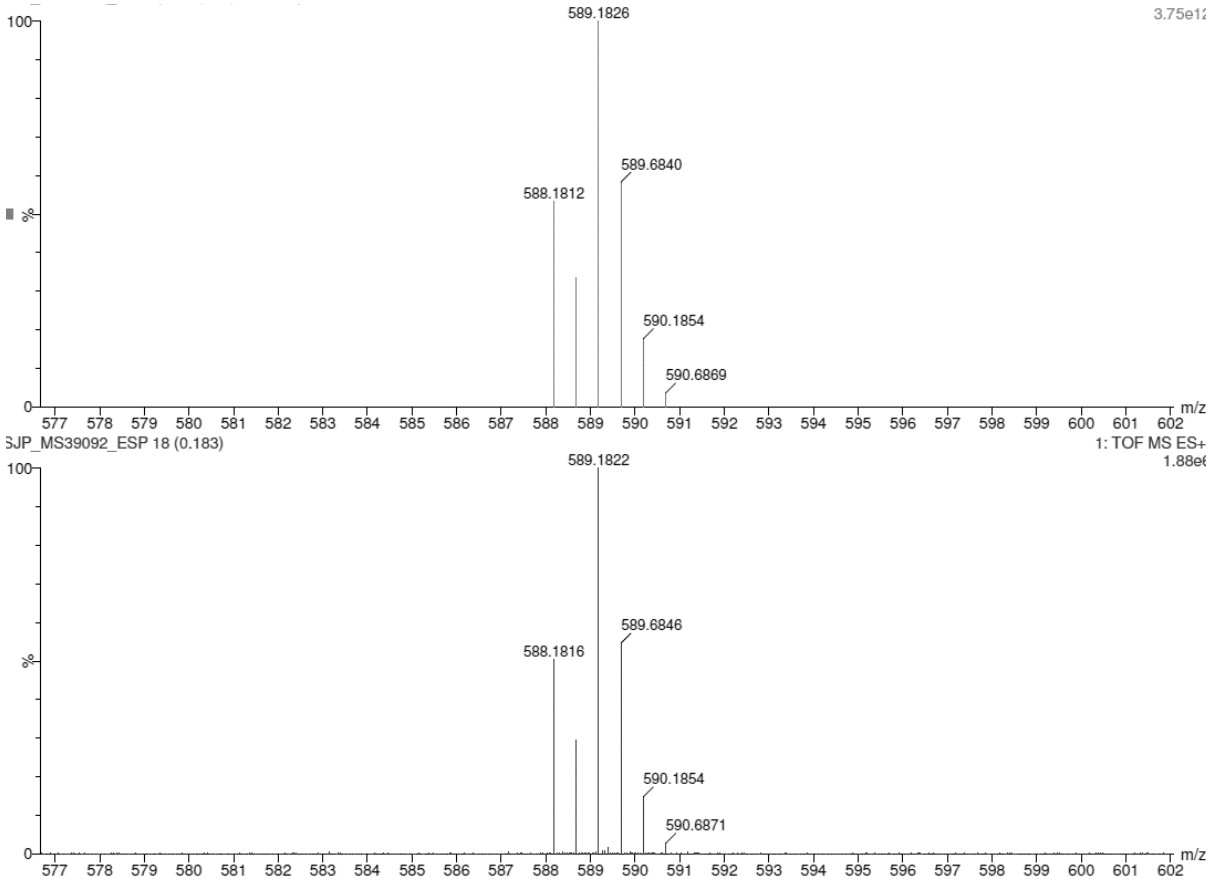

Figure S10. HRMS of $[Ir(Me_3quinox)_2(bipy\text{-}Im2)][PF_6]_3$ (ES+). (Top - theoretical; bottom - experimental).

S1.4 [Ru-Au][PF_6]$_3$

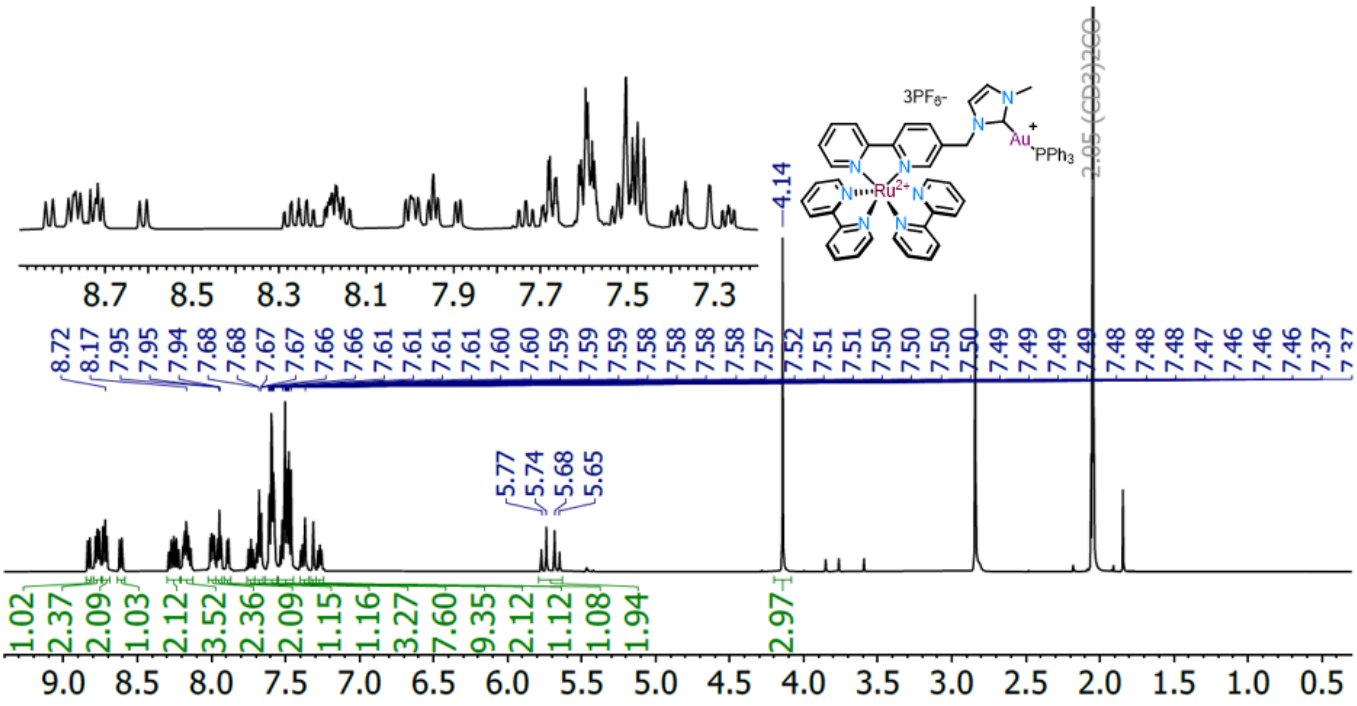

Figure S11. ^{1}H NMR spectrum of [Ru-Au][PF_6]$_3$ (500 MHz, 293 K, CD_3CN).

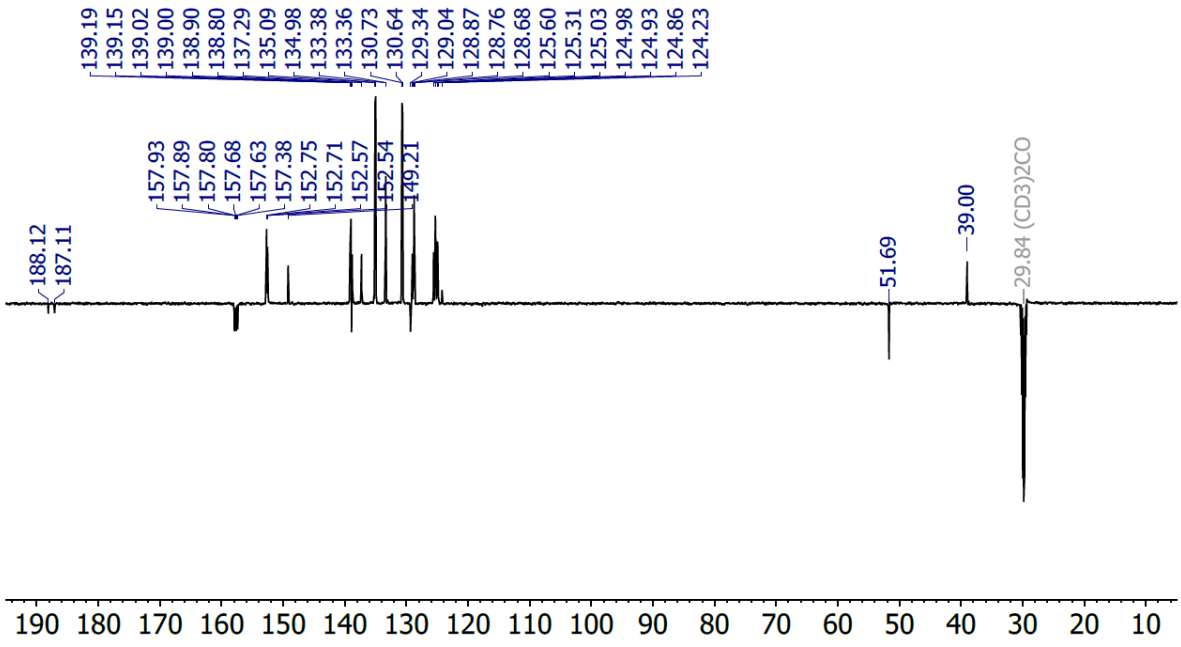

Figure S12. $^{13}C\{^{1}H\}$ NMR spectrum of [Ru-Au][PF_6]$_3$ (126 MHz, 293 K, CD_3CN).

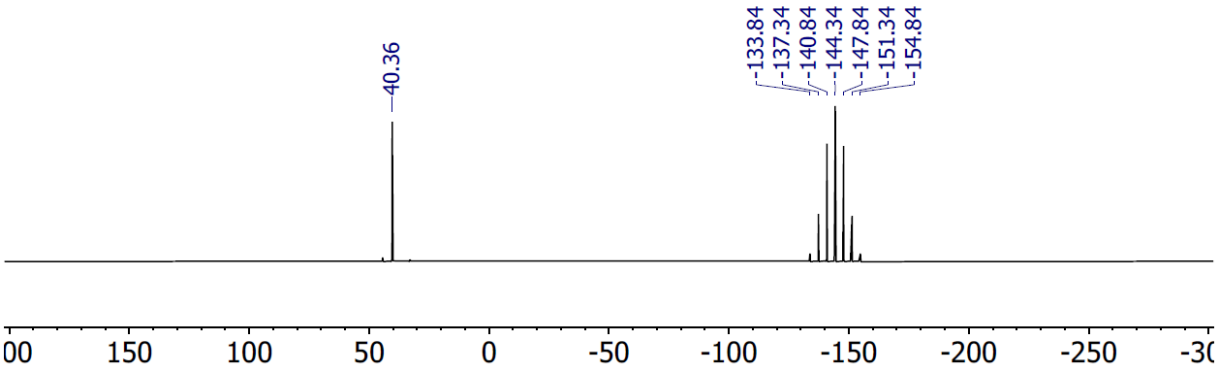

Figure S13. $^{31}P\{^{1}H\}$ NMR spectrum of [Ru-Au][PF_6]$_3$ (202 MHz, 293 K, CD_3CN).

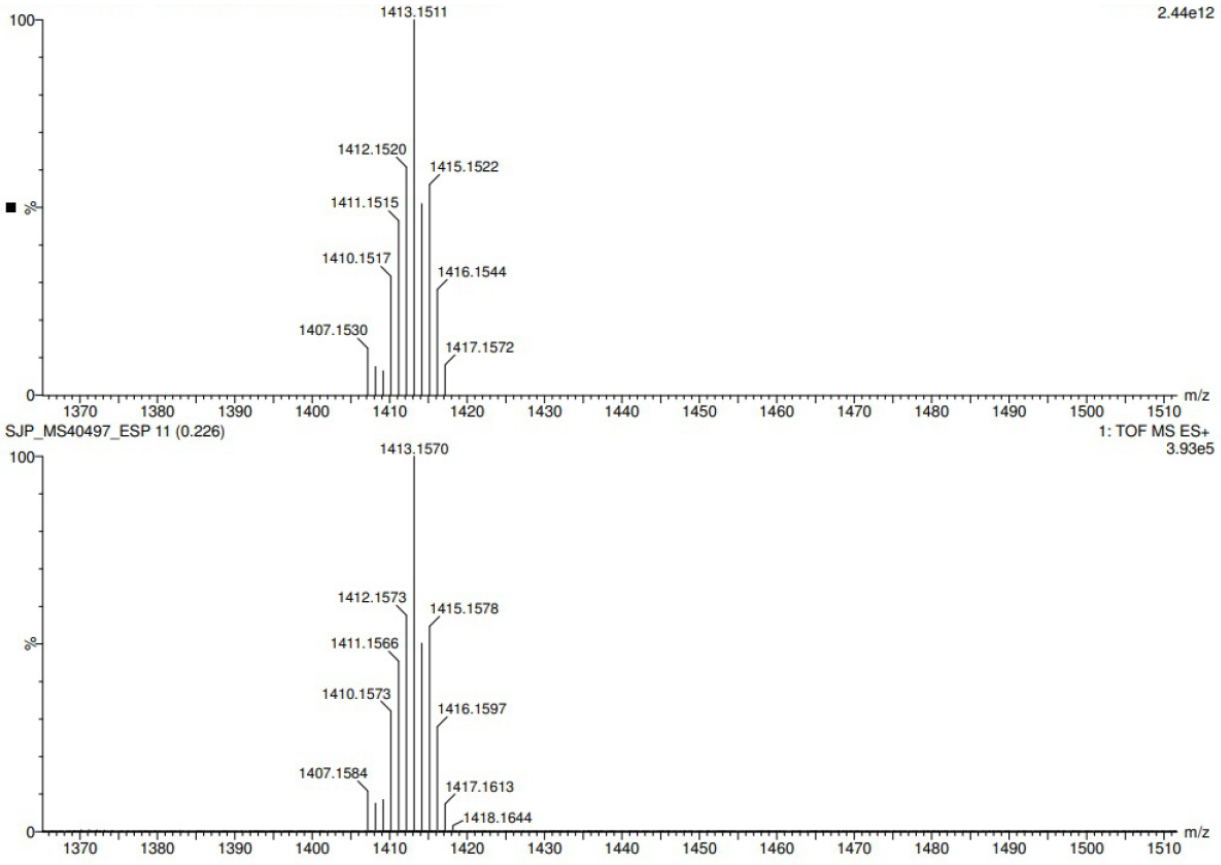

Figure S14. HRMS of [Ru-Au][PF_6]$_3$ (ES+). (Top - theoretical; bottom - experimental).

S1.5 $[Ru\text{-}Au_2][PF_6]_4$

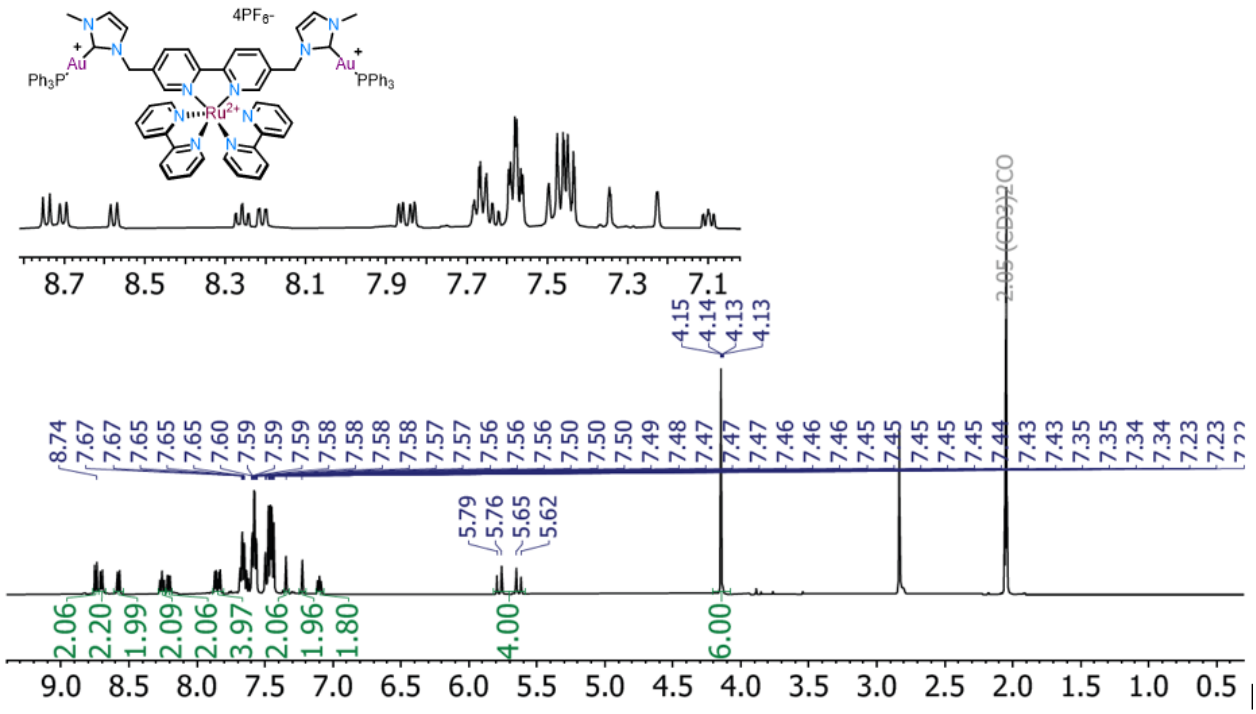

Figure S15. ^{1}H NMR spectrum of $[Ru\text{-}Au_2][PF_6]_4$ (500 MHz, 293 K, CD_3CN).

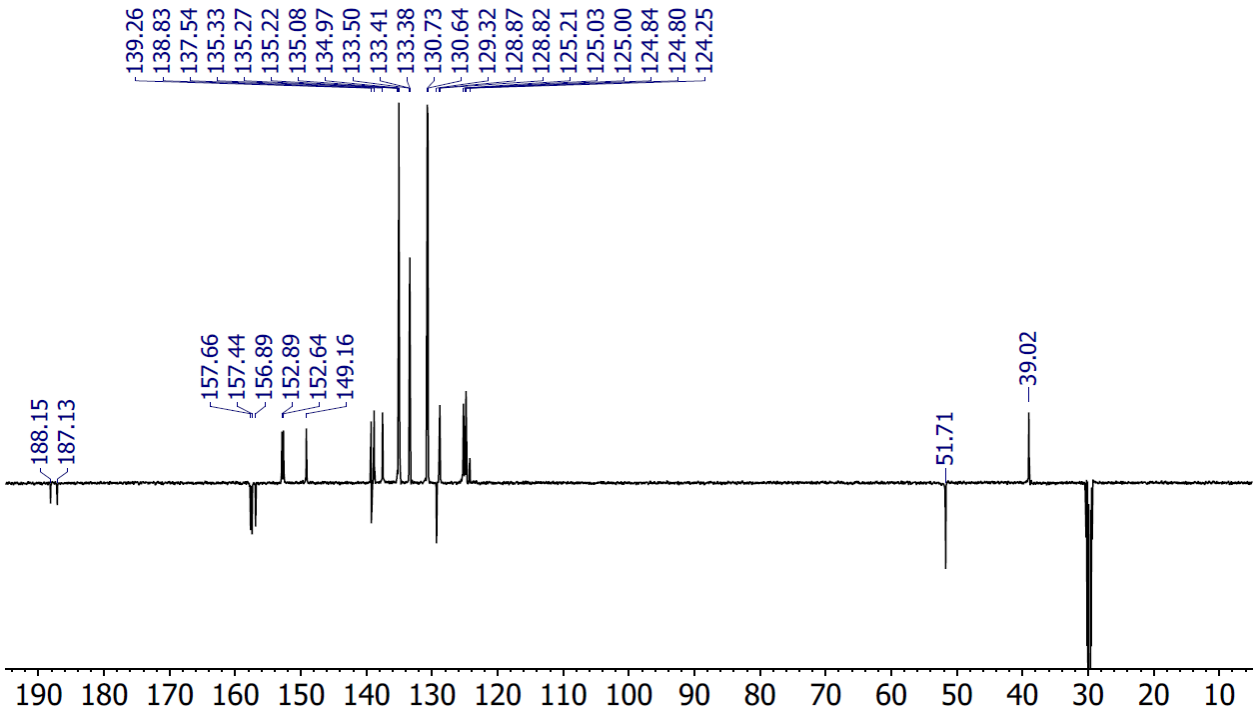

Figure S16. $^{13}C\{^{1}H\}$ NMR spectrum of $[Ru\text{-}Au_2][PF_6]_4$ (126 MHz, 293 K, CD_3CN).

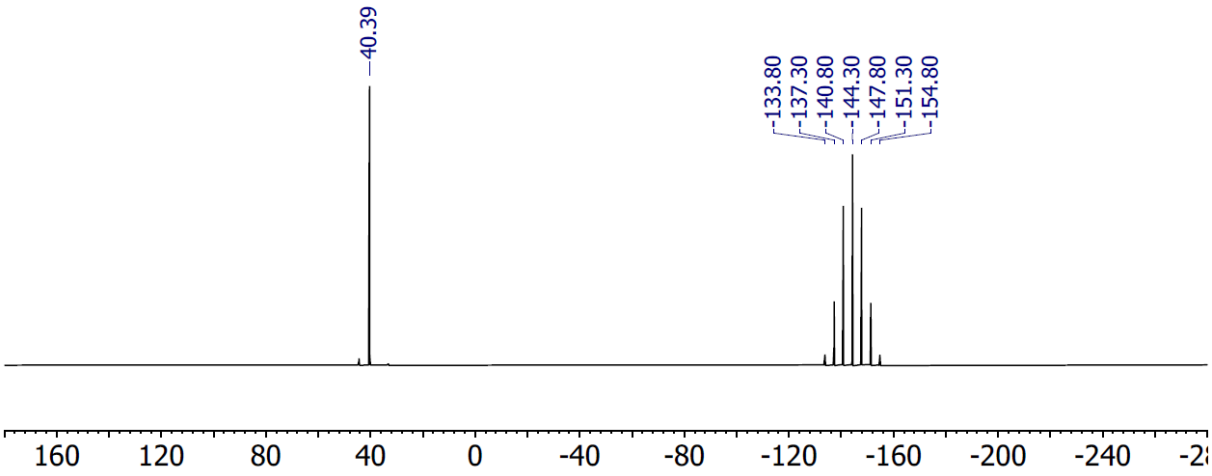

Figure S17. $^{31}P\{^{1}H\}$ NMR spectrum of [Ru-Au_2][PF_6]$_4$ (202 MHz, 293 K, CD_3CN).

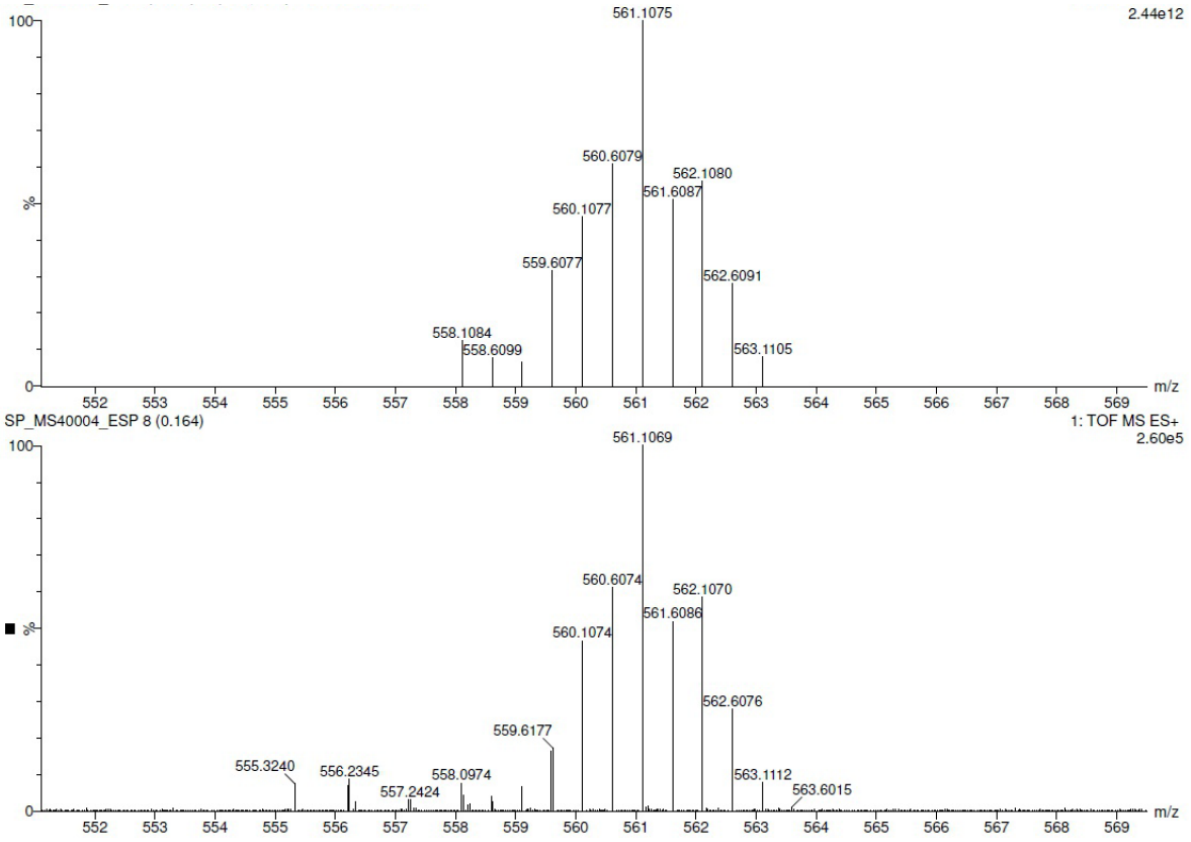

Figure S18. HRMS of [Ru-Au_2][PF_6]$_4$ (ES+). (Top - theoretical; bottom - experimental).

S1.6 [Ir-Au][PF_6]$_2$

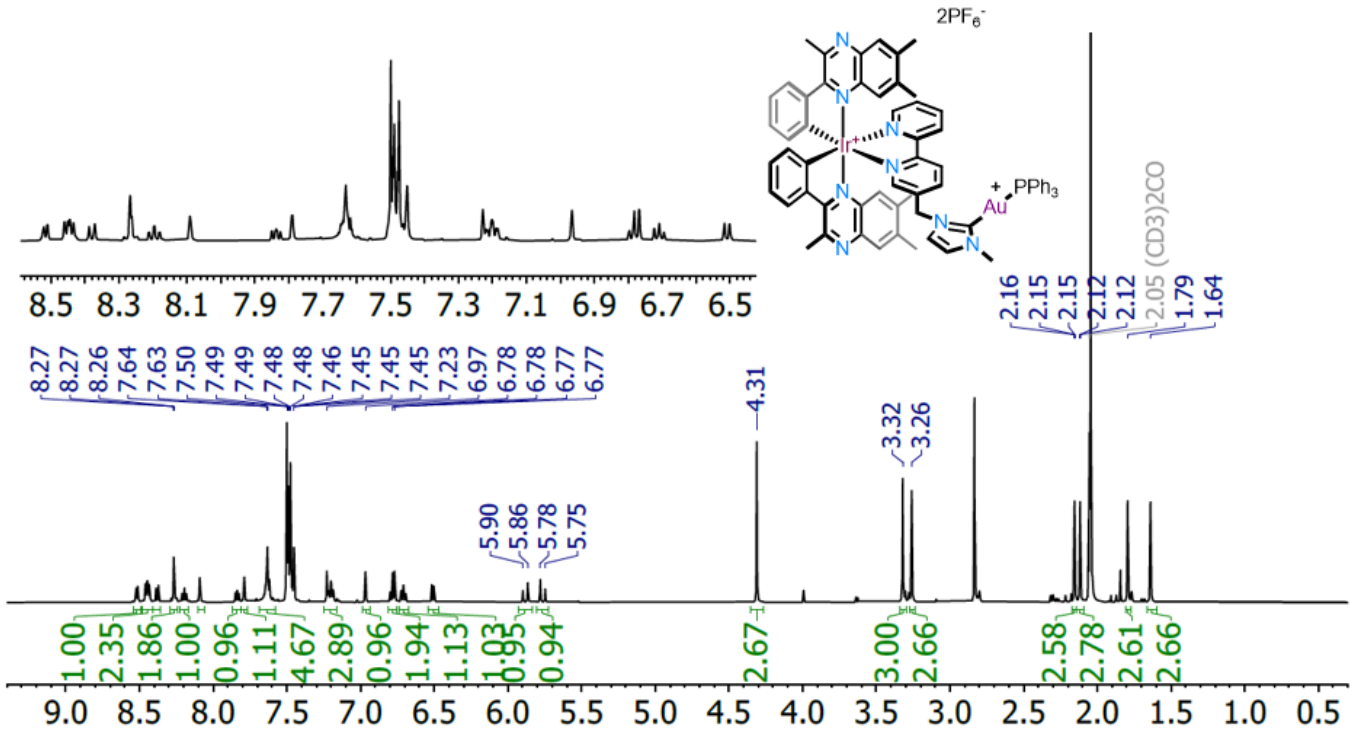

Figure S19. ^{1}H NMR spectrum of [Ir-Au][PF_6]$_2$ (500 MHz, 293 K, CD_3CN).

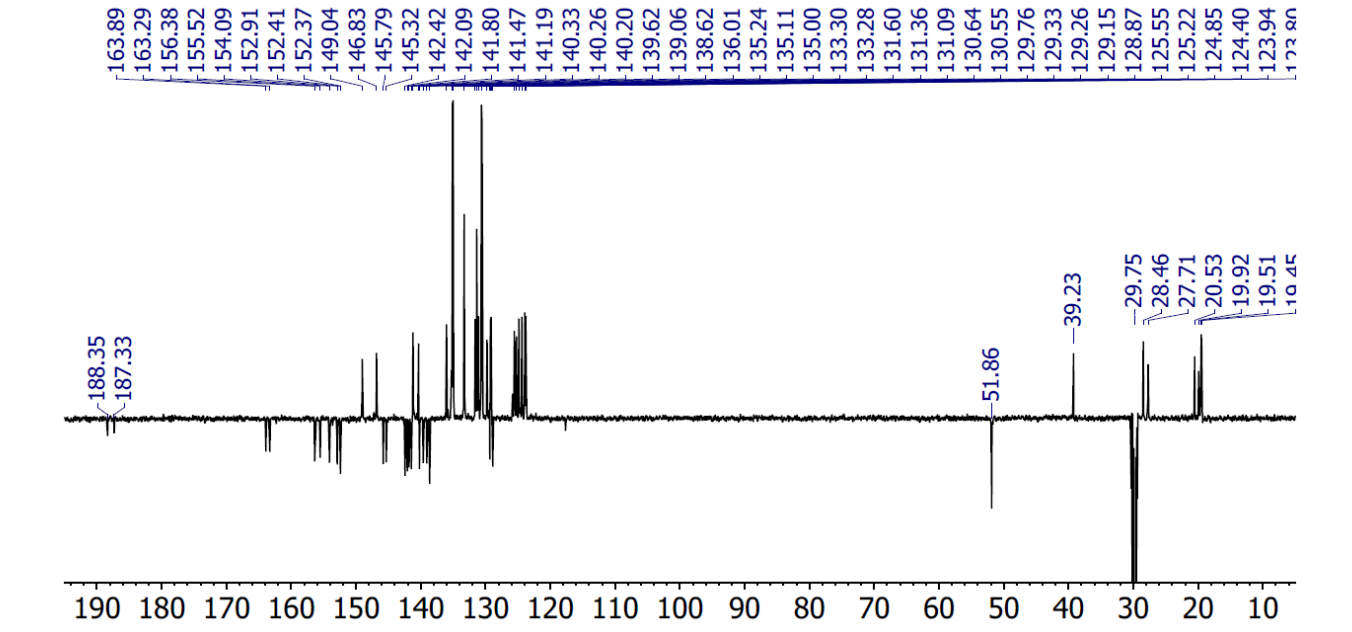

Figure S20. $^{13}C\{^{1}H\}$ NMR spectrum of [Ir-Au][PF_6]$_2$ (126 MHz, 293 K, CD_3CN).

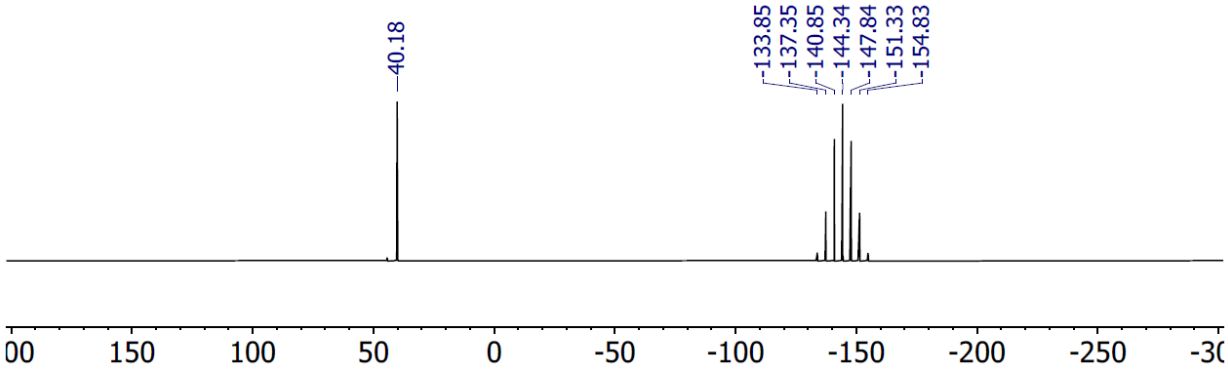

Figure S21. $^{31}P\{^{1}H\}$ NMR spectrum of [Ir-Au][PF_6]$_2$ (202 MHz, 293 K, CD_3CN).

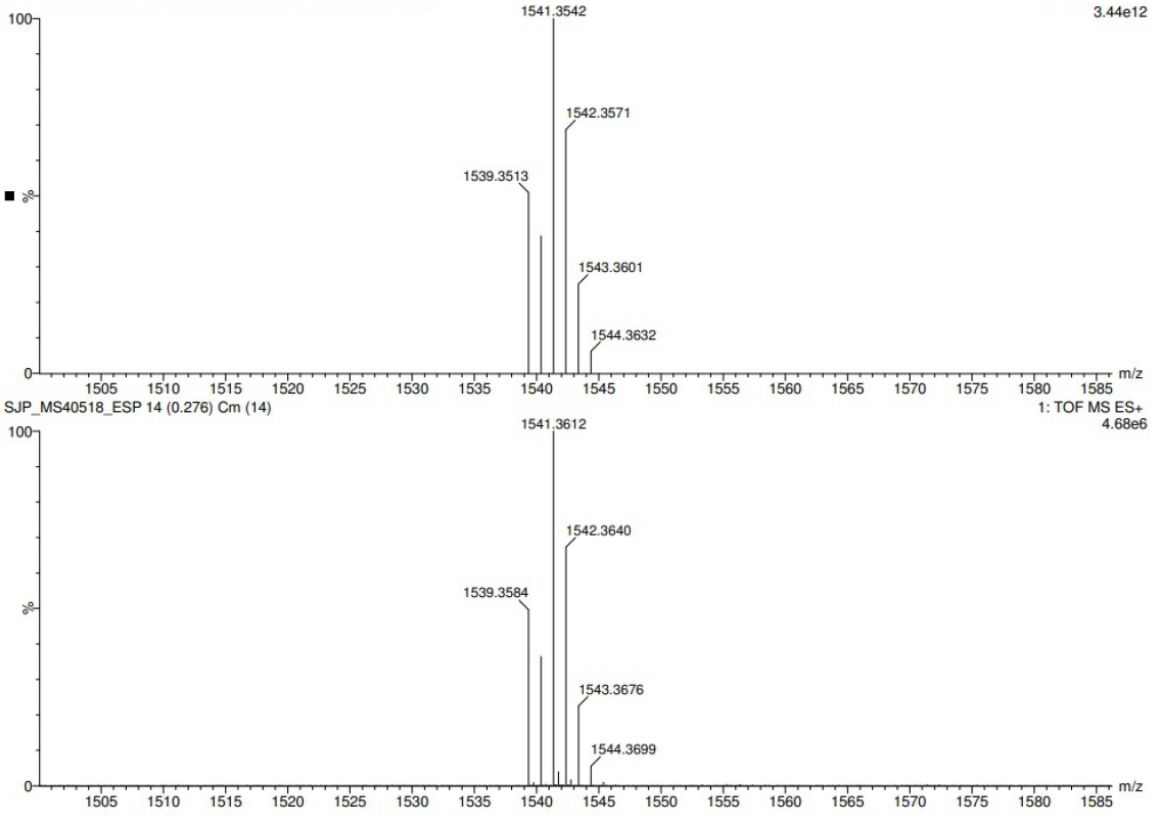

Figure S22. HRMS of [Ir-Au][PF_6]$_2$ (ES+). (Top - theoretical; bottom - experimental).

S1.7 [Ir-Au$_2$][PF$_6$]$_3$

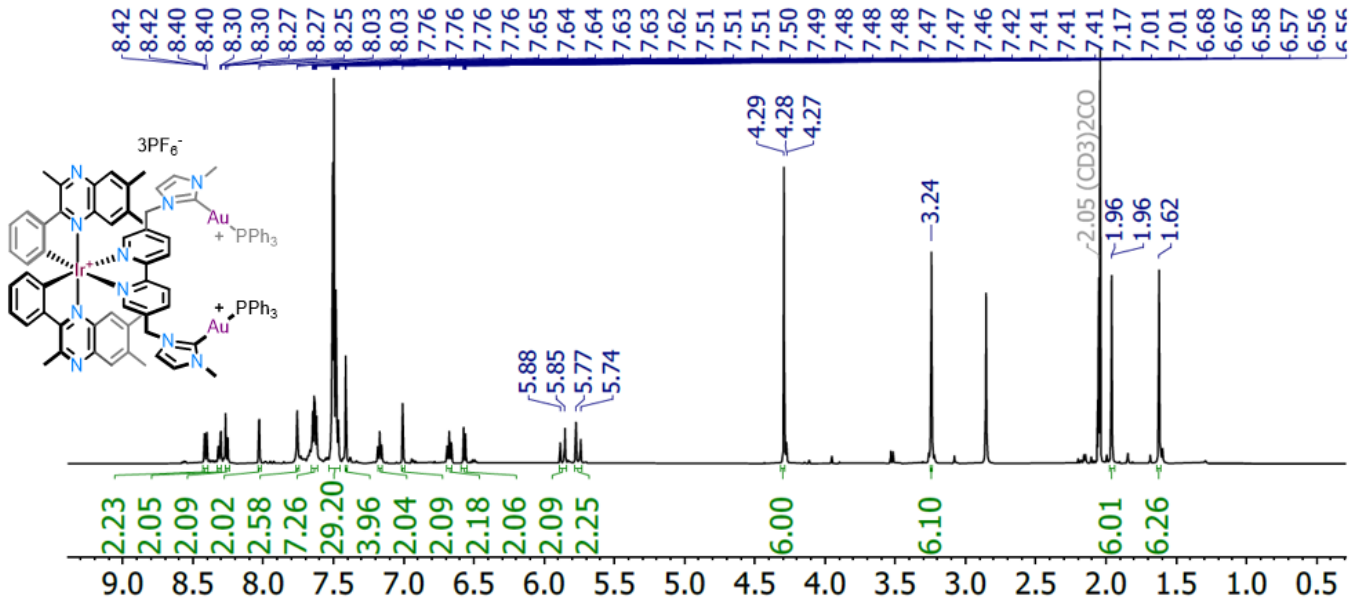

Figure S23. ^{1}H NMR spectrum of [Ir-Au$_2$][PF$_6$]$_3$ (500 MHz, 293 K, CD$_3$CN).

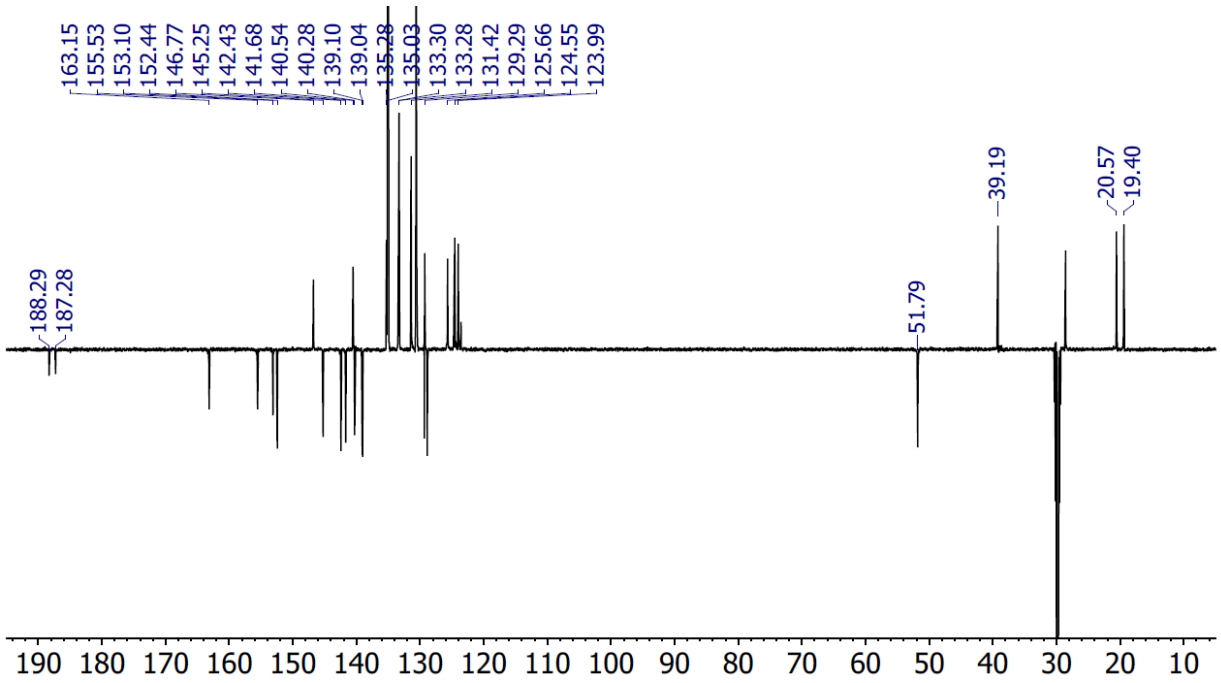

Figure S24. ^{13}C{^{1}H} NMR spectrum of [Ir-Au$_2$][PF$_6$]$_3$ (126 MHz, 293 K, CD$_3$CN).

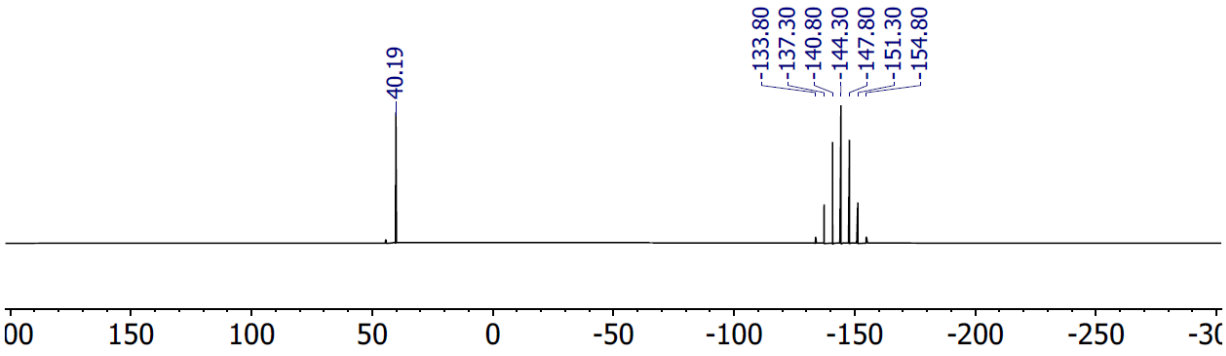

Figure S25. $^{31}P\{^{1}H\}$ NMR spectrum of [Ir-Au_2][PF_6]$_3$ (202 MHz, 293 K, CD_3CN).

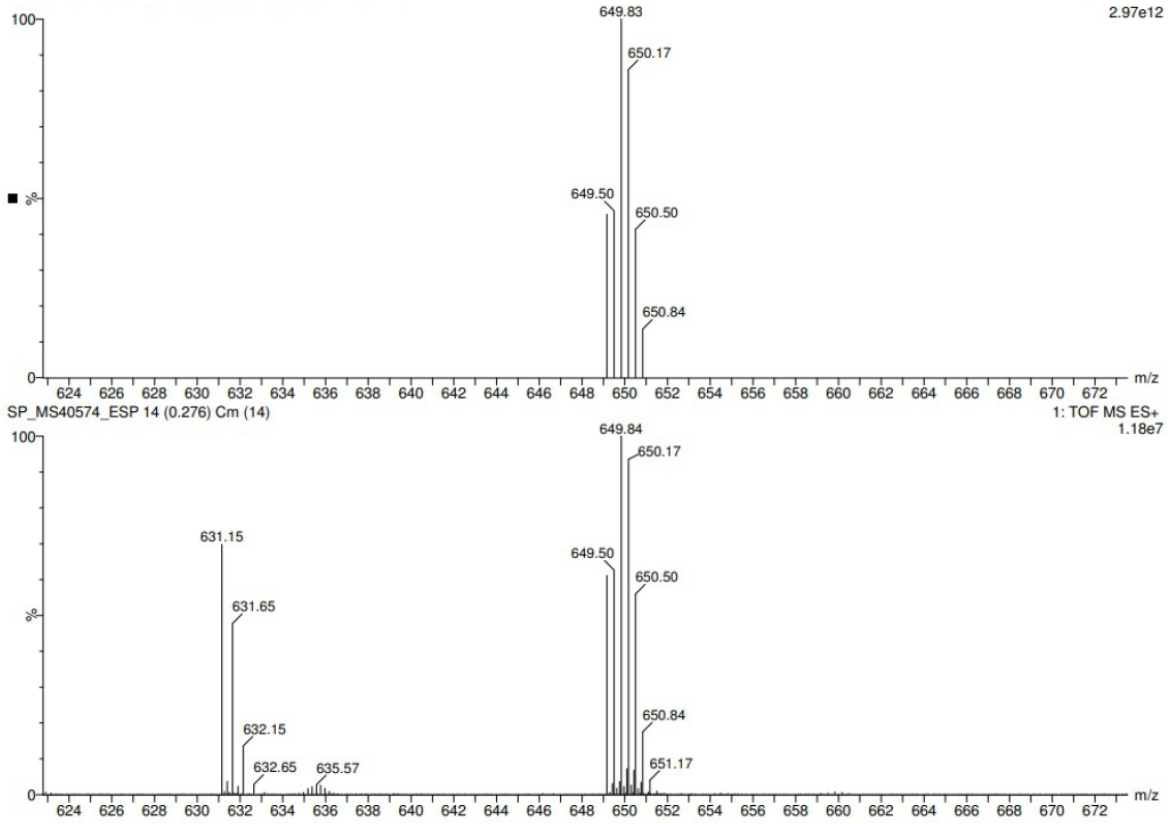

Figure S26. HRMS of [Ir-Au_2][PF_6]$_3$ (ES+). (Top - theoretical; bottom - experimental).

S2. Single-crystal X-ray crystallography

A suitable crystal was mounted on a glass fibre with Fomblin oil and collected at 150(2) K. The structure was solved using Olex2[1] and the ShelXT[2] structure solution program using Direct Methods and refined with the ShelXL[3] refinement package using Least Squares refinement.

S2.1 Structure of $[Ir(Me_3quinox)_2(MeCN)_2][PF_6]$

Table S1. Crystals data and structure refinement for $[Ir(Me_3quinox)_2(MeCN)_2][PF_6]$

Identification code	$[Ir(Me_3quinox)_2(MeCN)_2][PF_6]$
Empirical formula	$C_{38}H_{36}BF_4IrN_6$
Formula weight	855.74
Temperature/K	150
Crystal system	triclinic
Space group	P-1
a/Å	8.6524(4)
b/Å	12.6306(8)
c/Å	16.5547(10)
α/°	77.983(6)
β/°	78.821(5)
γ/°	85.964(5)
Volume/Å^3	1735.11(18)
Z	2
ρ_{calc}g/cm^3	1.638
μ/mm^{-1}	7.943
F(000)	848.0
Crystal size/mm^3	0.08 × 0.02 × 0.01
Radiation	Cu Kα (λ = 1.54178)
2Θ range for data collection/°	5.552 to 140.11
Index ranges	-10 ≤ h ≤ 8, -15 ≤ k ≤ 15, -20 ≤ l ≤ 20
Reflections collected	27371
Independent reflections	6455 [R_{int} = 0.1101, R_{sigma} = 0.0902]
Data/restraints/parameters	6455/0/460
Goodness-of-fit on F^2	1.071
Final R indexes [I>=2σ (I)]	R_1 = 0.0750, wR_2 = 0.1838
Final R indexes [all data]	R_1 = 0.1124, wR_2 = 0.2050
Largest diff. peak/hole / e Å^{-3}	2.08/-3.47

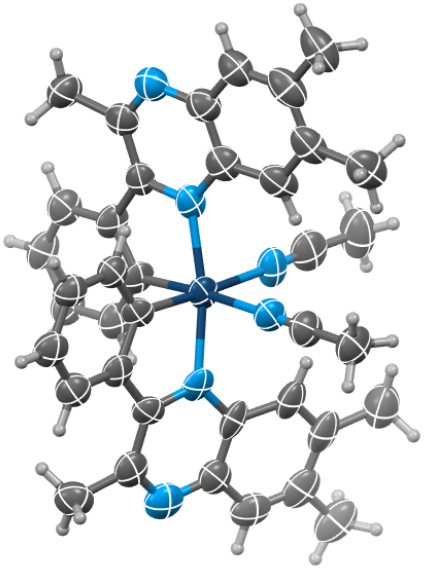

Figure S28. Single crystal X-ray structure of $[Ir(Me_3quinox)_2(MeCN)_2][BF_4]$ (ellipsoids plotted at the 50% probability level; H-atoms and counter anions omitted for clarity)

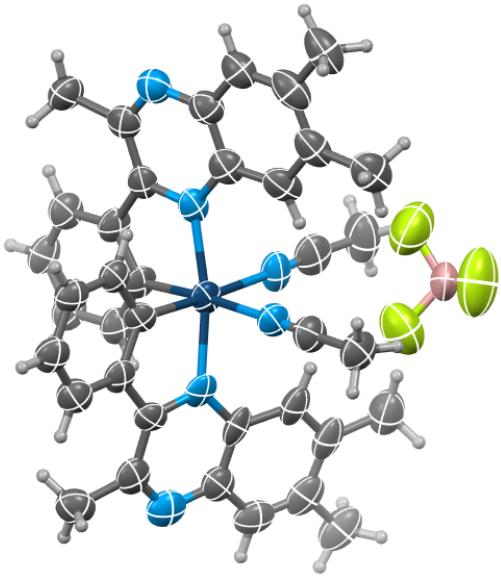

Figure S29. Single crystal X-ray structure of $[Ir(Me_3quinox)_2(MeCN)_2][BF_4]$ (ellipsoids plotted at the 50% probability level; counter anions omitted for clarity)

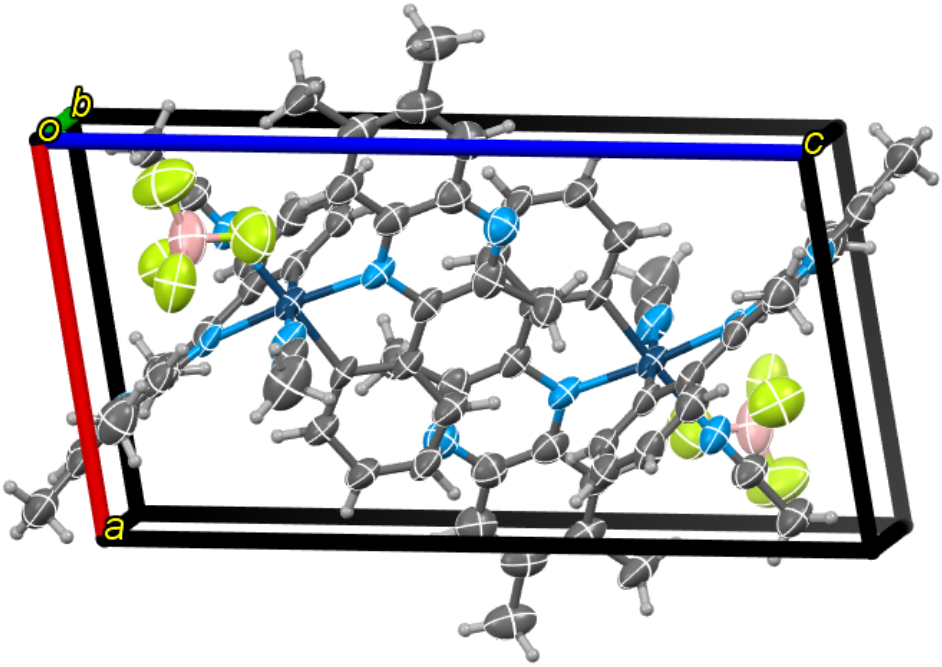

Figure S30. Unit cell packing of $[Ir(Me_3quinox)_2(MeCN)_2][BF_4]$ (ellipsoids plotted at the 50% probability level)

S2.2 Structure of $[Ir(Me_3quinox)_2(bipy\text{-}Im2)][PF_6]_3$

Table S2. Crystals data and structure refinement for $[Ir(Me_3quinox)_2(bipy\text{-}Im2)][PF_6]_3$

Identification code	$[Ir(Me_3quinox)_2(bipy\text{-}Im2)][PF_6]_3$
Empirical formula	$C_{54}H_{52}F_{18}IrN_{10}P_3$
Formula weight	1468.16
Temperature/K	100.15
Crystal system	triclinic
Space group	P-1
a/Å	16.5187(2)
b/Å	18.7439(3)
c/Å	22.3271(3)
α/°	105.1570(10)
β/°	108.1430(10)
γ/°	94.9750(10)
Volume/Å^3	6233.35(16)
Z	4
ρ_{calc}g/cm^3	1.564
μ/mm^{-1}	2.317
F(000)	2920.0
Crystal size/mm^3	0.12 × 0.1 × 0.025
Radiation	Mo Kα (λ = 0.71073)
2Θ range for data collection/°	4.406 to 57.398
Index ranges	-22 ≤ h ≤ 22, -25 ≤ k ≤ 25, -30 ≤ l ≤ 30
Reflections collected	170000
Independent reflections	32116 [R_{int} = 0.0806, R_{sigma} = 0.0667]
Data/restraints/parameters	32116/264/1628
Goodness-of-fit on F^2	1.032
Final R indexes [I>=2σ (I)]	R_1 = 0.0525, wR_2 = 0.1192
Final R indexes [all data]	R_1 = 0.0848, wR_2 = 0.1312
Largest diff. peak/hole / e Å^{-3}	3.72/-1.20

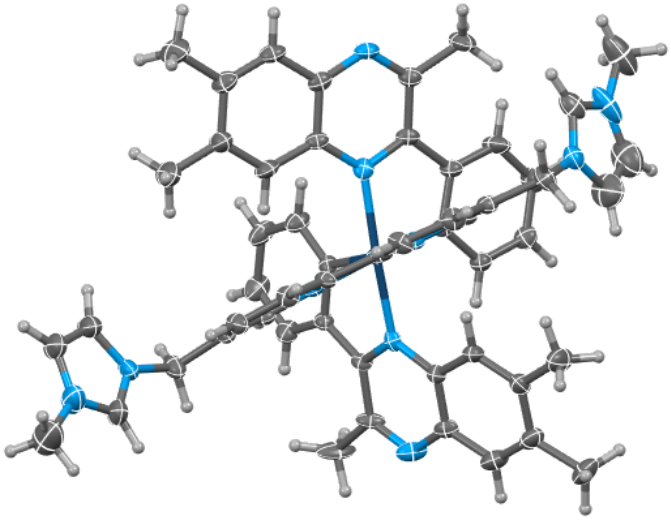

Figure S32. Single crystal X-ray structure of $[Ir(Me_3quinox)_2(bipy\text{-}Im2)][PF_6]_3$ (ellipsoids plotted at the 50% probability level; counter anions omitted for clarity)

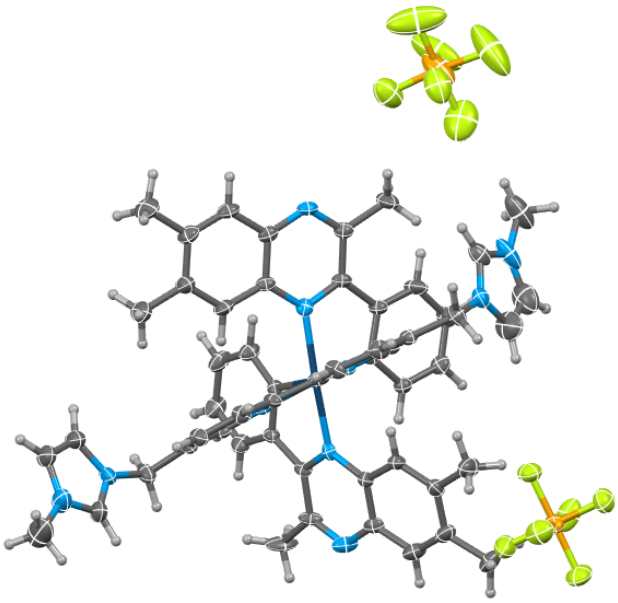

Figure S33. Single crystal X-ray structure of $[Ir(Me_3quinox)_2(bipy\text{-}Im2)][PF_6]_3$ (ellipsoids plotted at the 50% probability level)

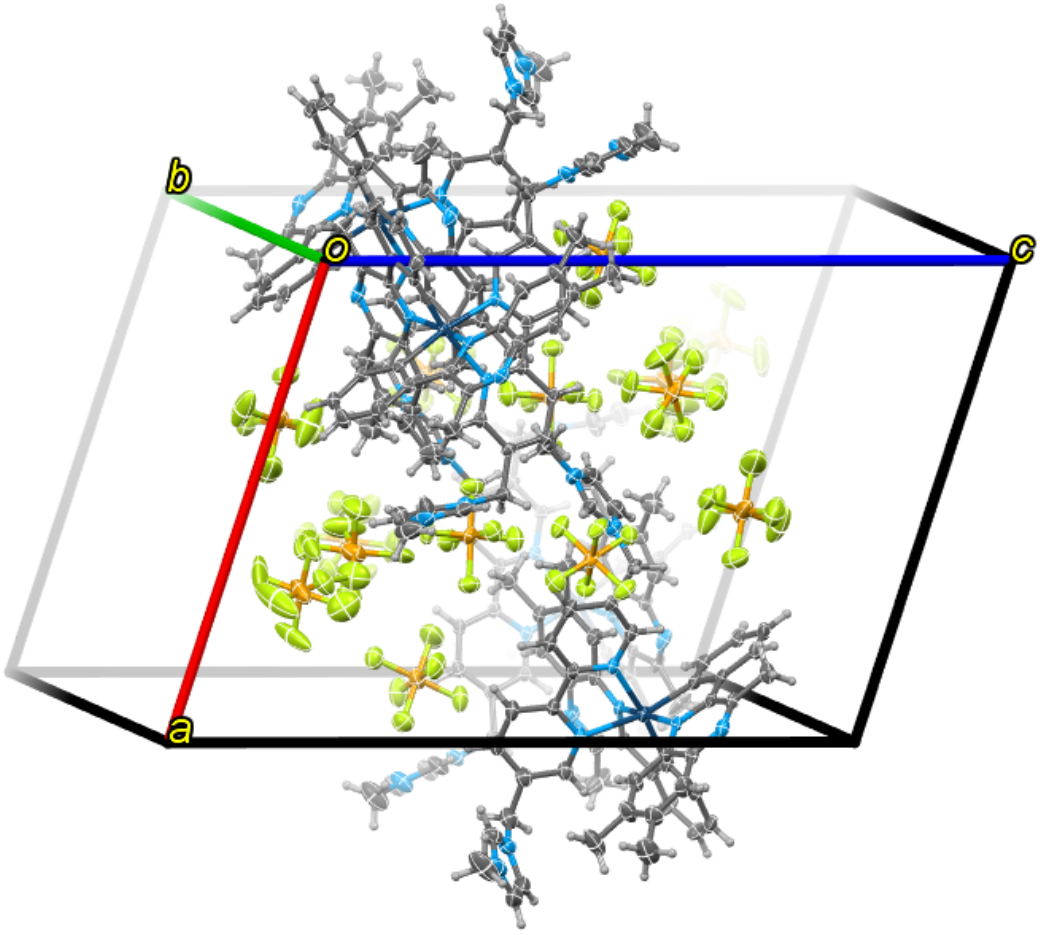

Figure S34. Unit cell packing of [Ir(Me_3quinox)$_2$(bipy-Im2)][PF_6]$_3$ (ellipsoids plotted at the 50% probability level)

S2.3 Structure of [Ru-Au][PF_6]$_3$

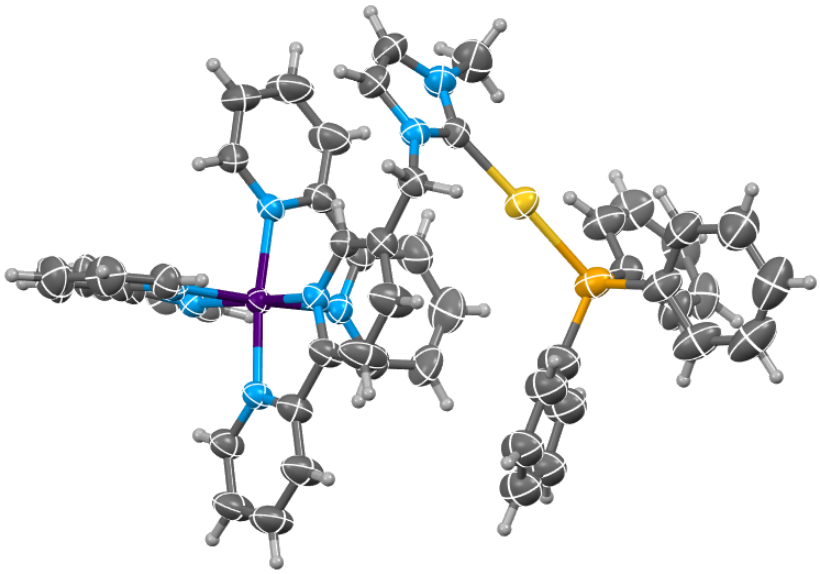

Figure S35. Single crystal X-ray structure of [Ru-Au][PF_6]$_3$ (ellipsoids plotted at the 50% probability level; counter anions and disorder omitted for clarity)

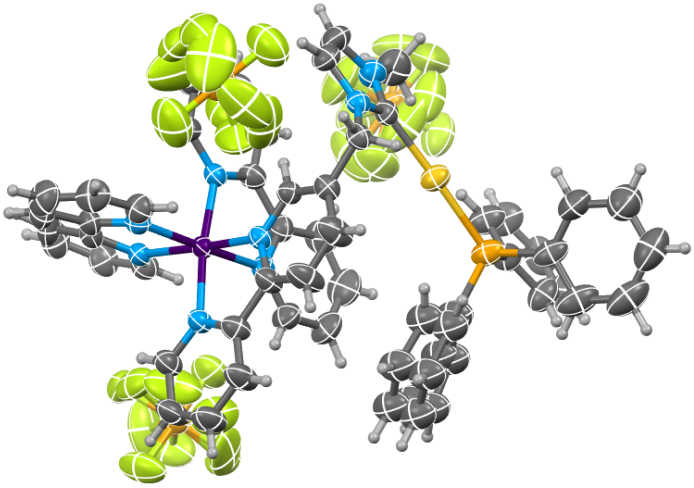

Figure S36. Single crystal X-ray structure of [Ru-Au][PF_6]$_3$ (ellipsoids plotted at the 50% probability level)

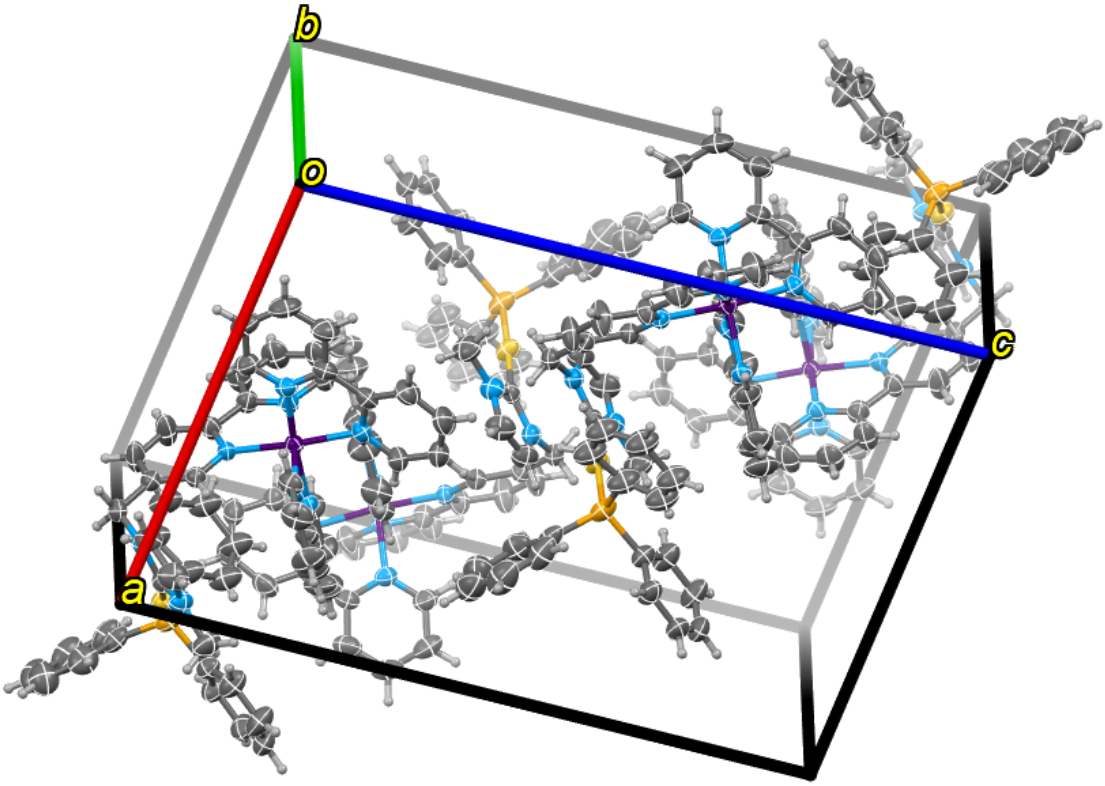

Figure S37. Unit cell packing of [Ru-Au][PF_6]$_3$ (ellipsoids plotted at the 50% probability level)

Table S3. Crystals data and structure refinement for [Ru-Au)][PF_6]$_3$

Identification code	[Ru-Au)][PF_6]$_3$
Empirical formula	$C_{53}H_{45}AuF_{18}N_8P4Ru$
Formula weight	1557.88
Temperature/K	293(2)
Crystal system	monoclinic
Space group	P1 2_1/n1
a/Å	13.5010(3)
b/Å	21.5970(4)
c/Å	20.6880(5)
α/°	90
β/°	98.515(2)
γ/°	90
Volume/Å^3	5965.70 (2)
Z	4
ρ_{calc}g/cm^3	1.735
μ/mm^{-1}	2.917
F(000)	2920.0
Crystal size/mm^3	0.46 × 0.21 × 0.07
Radiation	Mo Kα (λ = 0.71073)
2Θ range for data collection/°	6.864 to 59.83
Index ranges	-18 ≤ h ≤ 18, -29 ≤ k ≤ 29, -28 ≤ l ≤ 28
Reflections collected	62240
Independent reflections	32116 [R_{int} = 0.0806, R_{sigma} = 0.0667]
Data/restraints/parameters	15106/180/867
Goodness-of-fit on F^2	1.041

Final R indexes [I>=2σ (I)]	R_1 = 0.0373, wR_2 = 0.0735
Final R indexes [all data]	R_1 = 0.0738, wR_2 = 0.0874
Largest diff. peak/hole / e Å^{-3}	0.828/-0.820

Table S4. Bond metrics for [Ir(Me_3quinox)$_2$(bipy-Im2)][PF_6]$_3$ and [Ir(Me_3quinox)$_2$(bipy)][PF_6]

Atom numbers	[Ir(Me_3quinox)$_2$(bipy-Im2)][PF_6]$_3$	[Ir(Me_3quinox)$_2$(bipy)][PF_6][4]
	Bond lengths (Å) /Bond angles (°)	
Ir1-N_{bipy1}	2.207	2.176
Ir1-N_{bipy2}	2.166	2.168
Ir1-$N_{quinox1}$	2.064	2.090
Ir1-$N_{quinox2}$	2.077	2.067
Ir1-$C_{quinox1}$	1.982	1.991
Ir1-$C_{quinox2}$	2.006	2.014
N_{bipy1}-Ir1-$C_{quinox1}$	172.53	170.08
N_{bipy2}-Ir1-$C_{quinox2}$	167.16	170.96
$N_{quinox1}$-Ir1-$N_{quinox2}$	172.53	175.08

Table S5. Bond metrics for [Ru-Au]-[PF_6]$_3$

Atom numbers	[Ru-Au][PF_6]$_3$	[Ru(bipy)$_2$(bipy-Im2)][PF_6]$_4$[5]
	Bond lengths (Å) /Bond angles (°)	
Ru1-N2	2.071(3)	2.071
Ru1-N13	2.065(3)	2.086
Ru1-N14	2.057(3)	2.071
Ru1N25	2.051(3)	2.054
Ru1-N26	2.064(3)	2.060
Ru1-N37	2.039(3)	2.065
Au45-P46	2.2884(9)	
Au45-C43	2.034(3)	
N2-Ru1-N37	174.88(10)	175.66
N13-Ru1-N-14	173.68(11)	176.72
N25-Ru1-N26	173.17(11)	170.30
C43-Au-45-P-46	177.94(12)	

S3. Spectroscopy

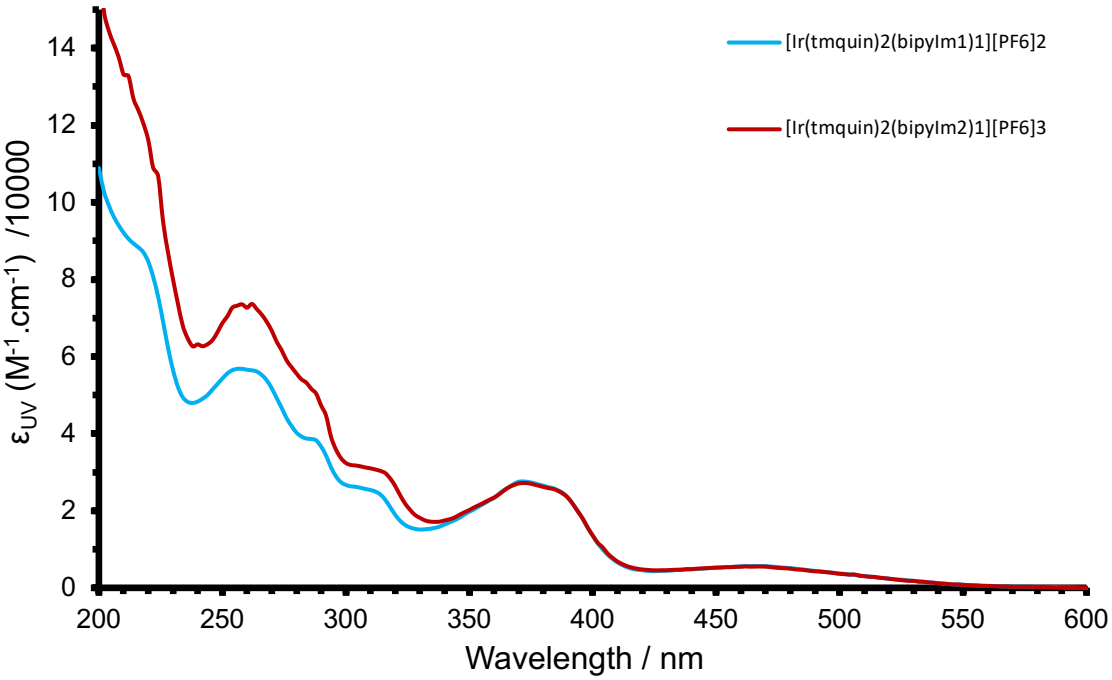

Figure S38. Absorption spectra for the polycationic iridium complexes (293 K, aerated MeCN, 10^{-5} M).

S4. Cyclic Voltammetry

Cyclic voltammetry was performed using a PalmSens4 potentiostat. Experiments were performed using HPLC grade MeCN with an analyte concentration of 1 mM at 293 K, using triply recrystallised [$^{n}Bu_4N$][PF_6] as the supporting electrolyte at 0.25 M concentration. A three-electrode setup was used, consisting of a platinum disc working electrode, a platinum wire counter-electrode and a silver wire pseudo-reference. Solutions were spared for 10 minutes with MeCN saturated stream of nitrogen gas. Voltammograms were referenced to the ferrocene/ferrocenium redox couple measured using the same conditions.

Table S6. Electrode oxidation potentials of the family of homo- and heterometallic complexes (mV shifts presented in parentheses)

Complex	Ox
[Ir(Me_3quinox)$_2$(bipy-Im1)][PF_6]$_2$	0.98 (100)
[Ir(Me_3quinox)$_2$(bipy-Im2)][PF_6]$_3$	0.99 (110)
[Ir-Au][PF_6]$_2$	1.01 (110)
[Ir-Au_2][PF_6]$_3$	1.04 (140)
[Ru-Au][PF_6]$_3$	0.93 (110)
[Ru-Au_2][PF_6]$_4$	0.94 (110)

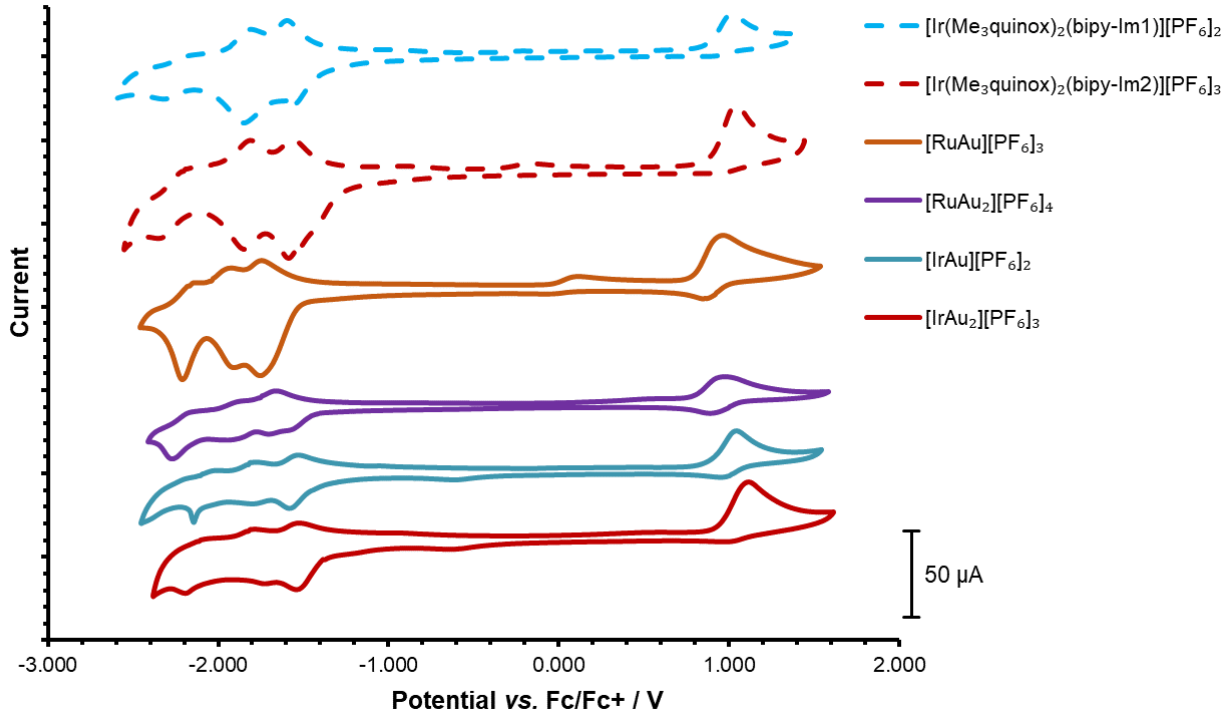

Figure S39. Cyclic voltammograms for the family of monometallic Ir/Ru heteropolymetallic Ir/Ru-Au complexes

S5. References

[1] O.V. Dolomanov, L.J. Bourhis, R.J. Gildea, J.A.K. Howard, H. Puschmann, *J. Appl. Cryst.*, 2009, **42**, 339-341.
[2] G.M. Sheldrick, *Acta Cryst*., 2015, **A71**, 3-8.
[3] G.M. Sheldrick, *Acta Cryst*., 2015, **C71**, 3-8
[4] K.A. Phillips, T.M. Stonelake, K. Chen, Y. Hou, J. Zhao, S.J. Coles, P.N. Horton, S.J. Keane, E.C. Stokes, I.A. Fallis, A.J. Hallett, S.P. O'Kell, J.B. Beames, S.J.A. Pope, Chem. Eur. J., 2018, 24, 8577
[5] R.C. Knighton, J.M. Beames, S. J. A. Pope, *Inorg. Chem*. 2023, **62**, 48, 19446–19456.